NET-PBH2: Negative Emissions Technology for Pale Blue Hydrogen

Western University

2024-06-30

Amarjeet Bassi, Joshua Pearce, Ying Zheng, Michael Boutlier

This project was supported by the financial contribution of the Independent Electricity System Operator.

This project is supported by the financial contribution of the Independent Electricity System Operator (IESO), through its Hydrogen Innovation Fund. However, the views, opinions and learnings expressed in this report are solely those of the Western University.

Table of Contents

1. Executive Summary

Hydrogen has the potential to be a significant player in the energy and electricity markets. Currently, however, only a low fraction of the produced hydrogen is used for these applications. Grey hydrogen from the fossil fuel industry has applications in ammonia production, refining operations and methanol synthesis. The commercial production of green (electrolytically produced) hydrogen is also not very significant and blue hydrogen (where the carbon is captured and removed for net zero carbon emissions) is also of growing interest. The main challenges facing the production of green and blue hydrogen include both (1) scaling up the production and (2) effectively transitioning from the carbon intensive approaches to a low carbon hydrogen production environment. The high cost of green and blue hydrogen production makes these approaches less competitive at this time.

In this project the goal and a single milestone was to investigate the feasibility of integrating green hydrogen from a PV-AEM (5 kW) electrolyzer with an innovative technology for blue hydrogen. The latter used a non-thermal Plasma Reactor (NTPR) to convert biogas into hydrogen with simultaneous biological carbon sequestration in a microalgal photobioreactor. The green and blue hydrogen combination is termed "Pale Blue Hydrogen". The single milestone was divided into four sub projects: (a) separate simulated biogas (methane and carbon dioxide mixture) into individual components using graphene and commercial membranes; (b) convert the methane into hydrogen and carbon black using the plasma technology; (c) produce green hydrogen using a solar powered PV-AEM electrolyzer supplied by the industrial partner Cipher Neutron; (d) Cultivate microalgae at different scales up to 20,000 L to demonstrate the capture of carbon dioxide and nutrients from wastewater (nitrogen and phosphorus). Finally an integrated setup was demonstrated where the methane from the membrane separation was supplied to the plasma reactor and the carbon dioxide to a bench scale photobioreactor on site at ISFAR-Western University London, Ontario.

The validity of the gas separation and hydrogen production from methane (blue hydrogen) with production of carbon black and carbon dioxide capture by microalgae was clearly demonstrated. The PV-AEM 5 kW electrolyzer was successfully operated to produce hydrogen. A lifecycle analysis to measure the carbon footprint of the green, blue and pale blue hydrogen was also carried out which clearly indicated the advantages of a renewable energy based approach in this system. Water recycling was also demonstrated and the capture of carbon using microalgae based bio-composite eco-plastic was demonstrated. Overall all goals in the single milestone were completed and the feasibility of taking this combined approach to the next steps was clearly established. The financial support of IESO and the in-kind support of Cipher Neutron to support this "disruptive" approach is highly valued.

2. Introduction and Goal

Green hydrogen or electrolytically generated hydrogen is being favoured due to its potentially net zero environmental impact. However, the need for a power source and potential large water requirements in scaled up systems are limiting its current applications. The hypothesis in this proposal was to mitigate these limitations in three ways; a) use a PV array to provide a renewable power source for the electrolyzer; b) produce blue hydrogen by converting a GHG i.e. methane to hydrogen and carbon black by investigating a plasma reactor (also powered by a PV array). The methane source is a simulated biogas mixture of carbon dioxide and methane. Thus a grapheme membrane system was evaluated to separate the methane and carbon dioxide and also to recycle the methane from the plasma reactor; and c) demonstrate the potential of microalgae cultivation in photo reactors and ponds. Since microalgae grow on carbon dioxide as a sole source of carbon and other nutrient from wastewater streams. The clean water can also be recycled from the microalgal system as all the nutrients are consumed by the microalgae. Therefore in this proposal a net negative hydrogen production system is produced by mixing the green and blue hydrogen streams, removing carbon and also reducing the water footprint. The proposal had one milestone: to investigate the feasibility and validity of the above hypothesis and also demonstrate an integrated system. These goals were successfully achieved. The single milestone was further sub-divided into four parallel sub- projects. The individual goals of each sub-project are first presented and then the methodologies, results and discussion are presented.

2.1 Subproject 1: membrane separation

The objective of the membrane separation unit sub-project was to use membrane technology to separate biogas into methane and carbon dioxide. The starting point for blue hydrogen production was "Simulate" biogas consisting of methane and carbon dioxide. This activity was led by Dr. Michael Boutilier and his team. The use of inhouse graphene membranes was compared with commercial membranes. The methane was the source material for sub- project 2 and the carbon dioxide was the potential source material for sub-project 4. For enhanced efficiency, graphene-based membranes were developed for this purpose. The feasibility of the graphene membranes was compared with conventional polymer membranes and the best option was used in the biogas separation unit. During the course of the project, to increase overall hydrogen yield, it was decided that an additional membrane separation unit would be installed downstream of the plasma reactor to separate the product hydrogen from unreacted methane, which is then recycled through the plasma reactor.

2.2 Subproject 2: Conversion of methane using plasma reactor to "blue" hydrogen and carbon black powder.

This activity was led by Dr. Ying Zheng and her team. The overall goals were to demonstrate both blue hydrogen production and carbon black production. The objective of this sub-project was to use plasma-induced energy to split methane (CH_4) to hydrogen. The plasma generator was powered by a portable solar power supply (sub-project 3). The mixture of produced hydrogen and unreacted methane was supplied to a graphene membrane for separation (Sub-project 1), where purified hydrogen was supplied to downstream and methane was recycled. The byproduct of solid carbon from methene splitting can be further utilized as electrode materials for other energy devices (e.g., batteries). The feasibility of the plasma-assisted methene splitting system was validated and its performance was characterized and optimized. Sinc the carbon is removed from the gas stream as carbon black this is a net negative carbon emission technology. The efficiency of the process was further investigated by membrane separation of remaining methane and hydrogen and recycle of the hydrogen/

2.3 Subproject 3: Green hydrogen production using PV- AEM electrolysis cell:

This activity was led by Dr. Joshua Pearce and in direct collaboration with external industrial partner Cipher Neutron who provided the 5 kW AEM electrolyzer. The PV system was designed and built in-house and the production of green hydrogen was investigated. Other objectives in this project were to design and build the PV system to interface with the plasma reactor (sub project 2) and a bench scale photo bioreactor (sub- project 4).

2.4. Sub project 4: Water recycling and nutrient and carbon dioxide removal using microalgae cultivation at 7 L, 500 L and 20000 L scale.

This activity was led by Dr. Amarjeet Bassi and his team. Dr. Bassi also contributed to LCA analysis in collaboration with Dr. Pearce and his team. The objectives of this project were to cultivate **Chlorella vulgaris**, a robust green microalgae on two waste streams (fertilizer- simulated by plant food) and insect frass waste. The microalgae absorb 1.8 Kg of carbon dioxide per Kg of algal dry weight, thus it was important to demonstrate growth of the algae in photobioreactors. The largest system was a pond (20,000 L) on site at ICFAR -Western University in Ilderton Ontario. All demonstrations were very successful. The growth of the microalgae was monitored, the removal of nutrients and the recycle of water was demonstrated at a practical scale.

3. Jurisdictional Scan

At the present time, hydrogen accounts for a very low fraction (less than 5%) of the global energy usage. In addition, currently, hydrogen is used mostly in the chemical industry (ammonia production, refining operations and methanol synthesis). A very low fraction (less than 1%) of hydrogen is generated from solar electrolysis (Green Hydrogen) and 99% is still supplied (as Grey Hydrogen) from fossil fuel based industries. Currently hydrogen production from these sources also results in significant carbon dioxide emissions (830 MTA, IEA statistics) . Since electrolysis will continue to be a small fraction of the requirement for hydrogen demand in the near future, it is quite important that low carbon alternatives for hydrogen continue to be investigated and demonstrated. The current major bottlenecks for clean hydrogen include both (1) scaling up the production and (2) effectively transitioning from the carbon intensive approaches to a low carbon hydrogen production environment Another significant economic challenge is the high cost of hydrogen production which cannot compete effectively with competing energy sources. An analysis by IEA (2019) showed that Green hydrogen and Blue hydrogen costs are 2 to 4 times more than Grey hydrogen (from fossil fuels). Another limitation is the low productivity of electrolysis systems compared to Grey hydrogen production and the requirements for large volumes of fresh water (ca, 20 Kg H_2O/ Kg water for AEM elctrolysers) . The low energy density of hydrogen also makes it expensive to transport and store. Even though green hydrogen is not currently competitive, new combined approaches offer great potential. In this project, we investigated first the feasibility, then validated and tested an innovative combined approach which utilizes both green hydrogen (obtained by solar based water electrolysis) with blue hydrogen (methane conversion to hydrogen and carbon black and with carbon dioxide sequestration in a microalgal based bioplastic). We term this combined approach "Pale Blue" Hydrogen. In our view, we speculate that thiss approach adds economic value via a lowered water footprint, byproducts for commercial application from microalgae) and significantly lowered and potentially negative emissions (as carbon is stored for a long term). This single milestone or feasibility study was completed in the given one year time frame.

4. Approach/Methodology and Assumptions

The methodology for each sub-project is presented below.

4.1 Subproject 1: membrane separation

Membrane separation unit development involved membrane fabrication, performance characterization through gas permeance and selectivity measurements, and final unit integration into the demonstration system.

4.1.1 Graphene membrane fabrication

Graphene membranes were designed and fabricated for gas separation. Several designs were explored, but we settled on two promising designs to devote most of our effort toward.

Design 1 consists of single layer graphene over a porous polyimide support, with tears sealed by nylon plugs and selective pores created by brief oxygen plasma exposure. The fabrication steps are shown in Fig. 4.1-1A. Chemical vapour deposited graphene on copper is coated with a supporting poly(methyl methacrylate) layer by spin coating. The copper is etched away in ammonium persulfate. The graphene is then scooped onto a porous polyimide support for mechanical strength. The advantage of this support layer is that it is solvent resistant, facilitating the subsequent removal of the poly(methyl methacrylate) layer by submersion in acetone. The membrane is then exposed to oxygen plasma for 5 s. Tears in the membrane are sealed by exposing it on either side to adipoyl chloride and hexamethylene diamine (Fig. 4.1-1C), which form thin nylon plugs where they meet. A photograph of a membrane of this type is presented in Fig. 4.1-1B.

Design 2 consists of graphene with a flow rate resistance matching nanoporous carbon layer on top, supported underneath by a porous polycarbonate layer. The steps to make these membranes are outlined in Fig. 4.1-1E. Graphene on copper is coated with a nanoporous carbon layer by spin coating followed by annealing. The copper is then etched away in ammonium persulfate and the graphene scooped onto a porous polycarbonate layer for mechanical support. A scanning electron microscope image of the porous carbon layer overtop graphene is presented in Fig. 4.1-1D. Graphene membranes were successfully fabricated and further refinement and optimization continues.

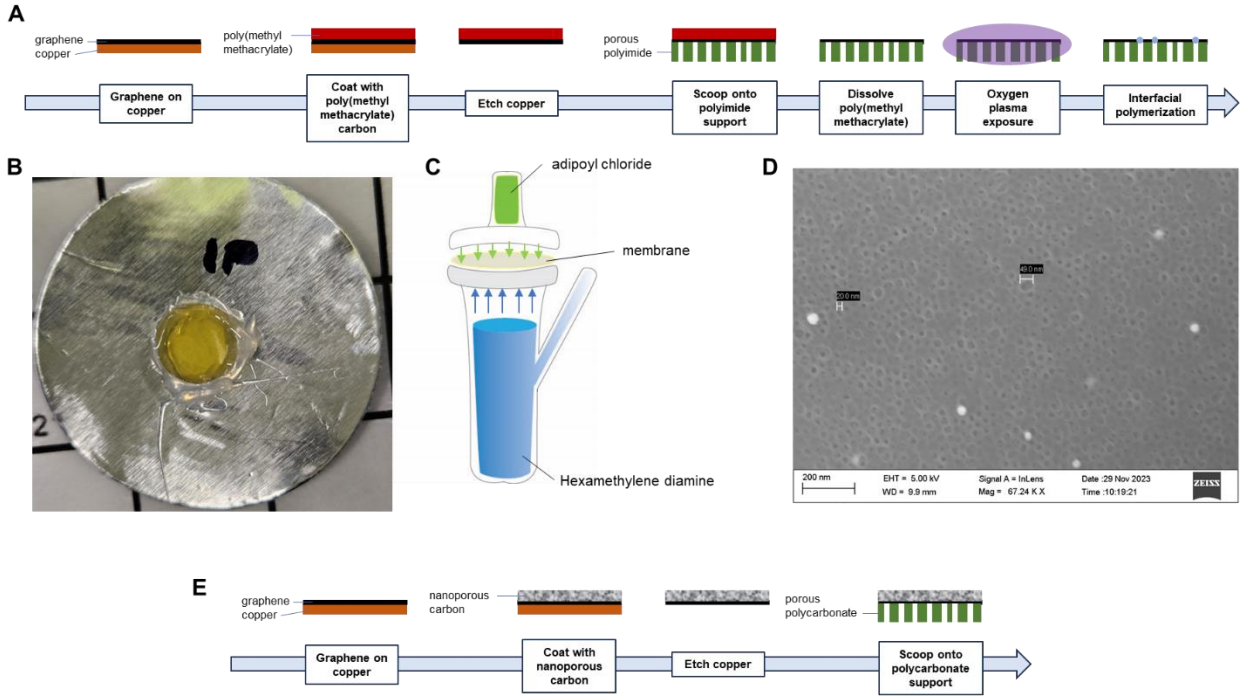

Fig. 4.1-1. Graphene membrane fabrication. (A) Fabrication steps for membrane design 1. (B) Photograph of fabricated membrane design 1. (C) Interfacial polymerization process. (D) Scanning electron microscope image of membrane design 2. (E) Fabrication steps for membrane design 2.

4.1.2 Membrane permeance and selectivity measurement

The gas permeance and selectivity of the graphene membranes were measured in custom-built gas permeation cells. Initially, this was done using a dead-end filtration system and single component gases.

The dead-end filtration system is shown in Fig. 4.1-2A,B. The upstream side of the membrane is flushed and then pressurised with a single component gas. The downstream side is pumped to remove air, and then sealed. The pressure rise on the downstream side over time as gas flows across the membrane is measured and used to compute flow rates. Fig. 4.1-2C shows an example characterization of a membrane.

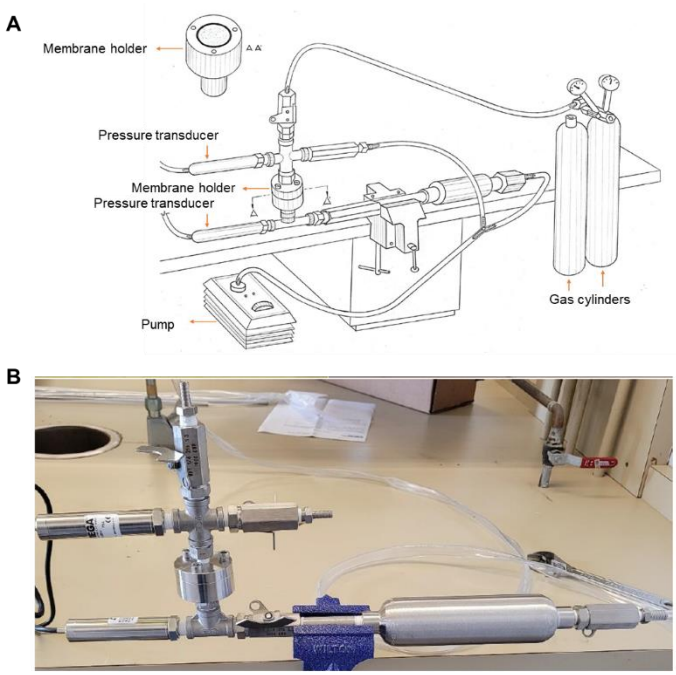

Fig. 4.1-2. Dead-end filtration membrane gas permeation cell. (A) Schematic. (B) Photograph.

To measure multi-component gas separation, which includes permeance interference effects between gas components, a cross-flow membrane permeance module was designed and constructed for membrane testing. A schematic of the design is presented in Fig. 4.1-3. The target separation for the project is methane/carbon dioxide at the 60%/40% composition of biogas. Cylinders of these gases connect upstream, with precise flow rates controlled by mass flow controllers to achieve the desired composition. A static mixer ensures that a uniform composition reaches the membrane. The upstream pressure is controlled by a needle valve and back-pressure regulator.

The system is configured to interchange different formats of membrane modules. For graphene membrane testing, two of the modules designed to hold these membranes are shown in Fig. 4.1-4. Hollow-fiber membrane modules, as pictured in Fig. 4.1-5, can also be connected. Argon sweep gas is connected to both the upstream and downstream side of the membrane. The three-way valves and check valves divert retentate and permeate streams to the gas chromatograph and volume flow meter to measure permeance and selectivity. Fig. 4.1-5 shows photographs of the constructed cross flow gas separation membrane system.

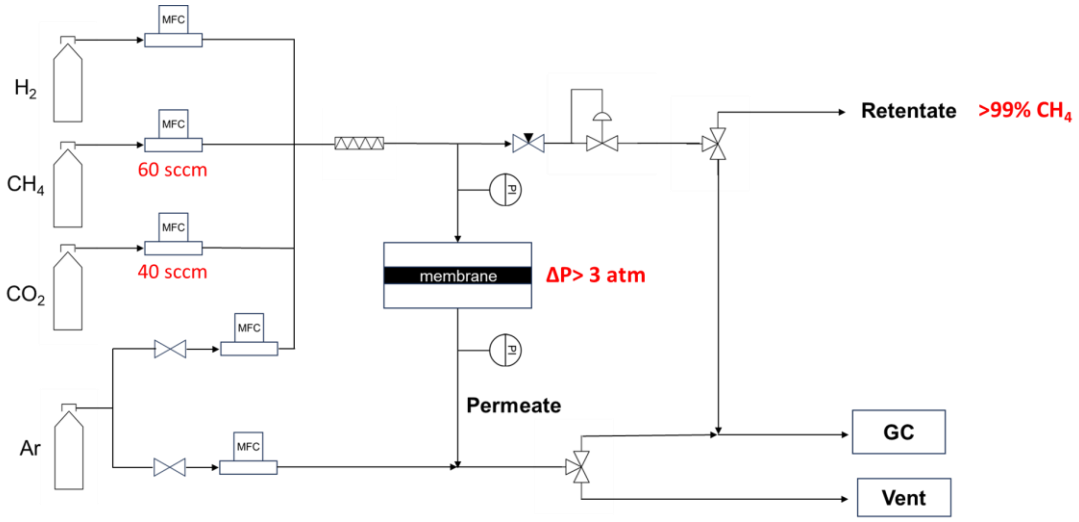

Fig. 4.1-3. Schematic of cross-flow gas separation membrane module.

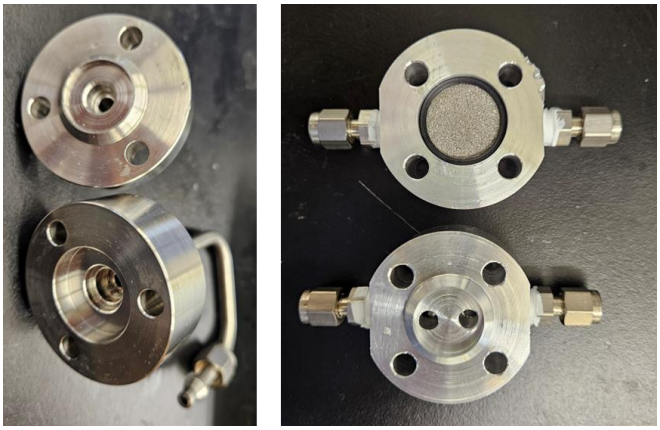

Fig. 4.1-4. Graphene membrane holder. (left) two-port holder. (right) four-port holder.

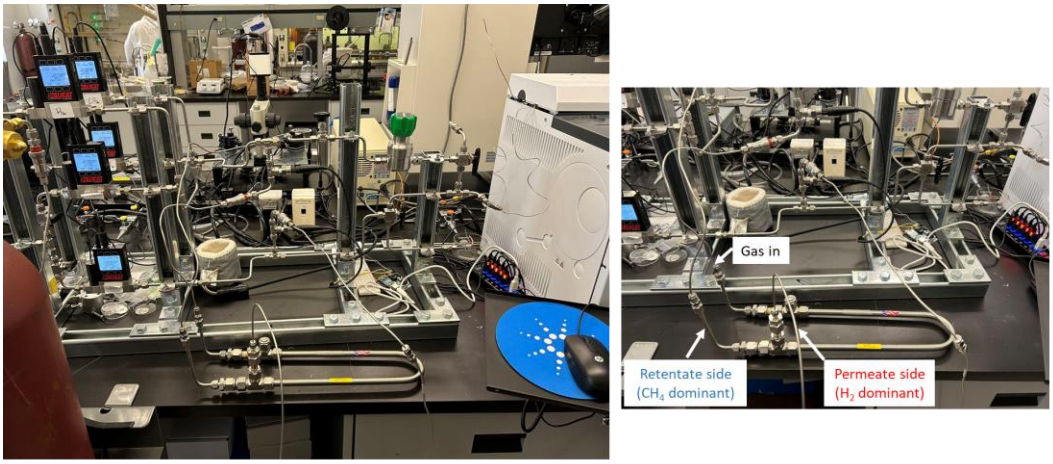

Fig. 4.1-5. Photograph of cross-flow gas separation membrane system with hollow-fiber membrane module connected.

4.2 Subproject 2: Plasma-assisted methene splitting for hydrogen production

Plasma-assisted methene splitting unit involves the design and fabrication of a plasma reactor and a plasma-based test system, the performance evaluation and optimization through gas chromatography measurements and gas conversion calculations, as well as the final unit integration into the overall demonstration system.

4.2.1 Design of plasma reactor and plasma-based test system

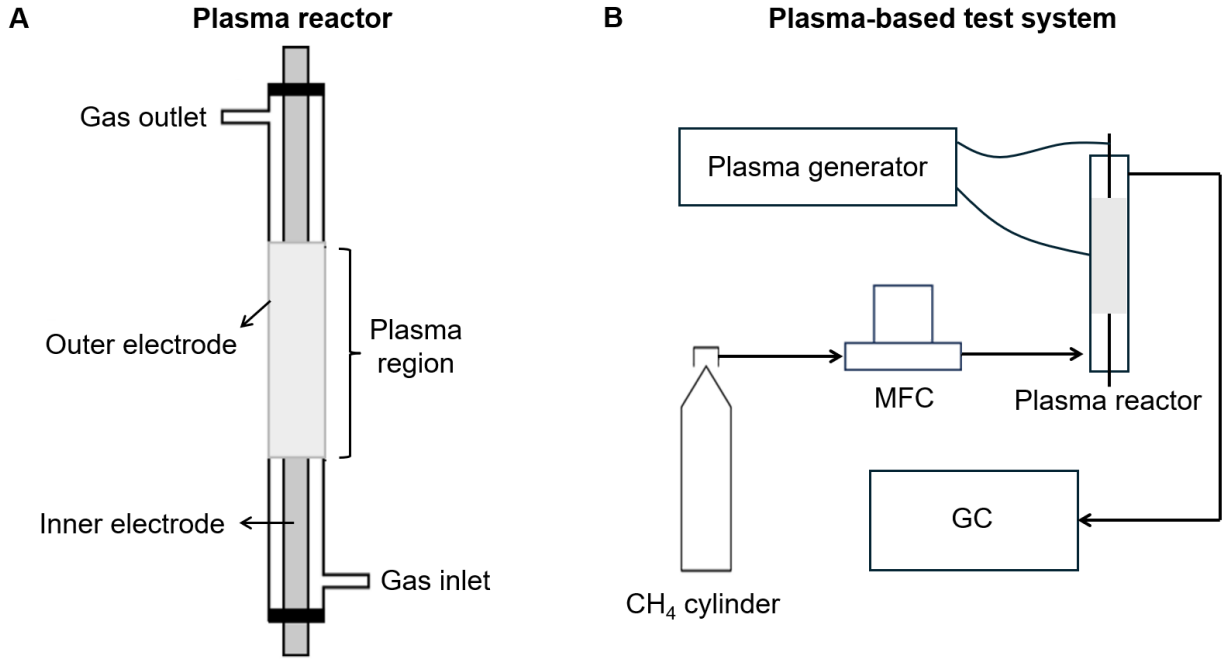

Fig. 4.2-1. Schematic of the as-designed plasma reactor (A) and plasma-based test system (B).

The basic configuration of the plasma reactor was designed as Fig. 4.2-1A. Due to the relatively simple structure and mild operation requirements (e.g., normal atmospheric pressure, low operation temperature), dielectric-barrier discharge (DBD)-type plasma reactor is selected. The main body of the reactor is a glass-made tube (dielectric material), attached with two small tubes as the gas inlet and outlet. The two ends of the main tube (top and bottom) are sealed by Teflon tape and vacuum silicone grease after inserting the copper-made inner electrode bar. The main tube is then covered by a steel-made mesh as the outer electrode. Preliminary reactor parameters are set as follows: the ID of the reactor main tube is 1.5 cm, the OD of the inner electrode is 1.2 cm, and the length of the outer electrode is 2-10 cm. This length further determines the length of the as-generated plasma region in the tube.

Furthermore, the plasma-based test system was designed as Fig. 4.2-1B. The CH_4 cylinder is used as the source of the input gas. The gas flowrate is controlled by a mass flow controller (MFC). Then, the well-controlled CH_4 flow is input to the plasma reactor at the inlet, flowing through the plasma region, and flowing out at the outlet. After connecting the two electrodes of the plasma

reactor with the plasma generator, the plasma state will be generated inside the reactor tube to interact with CH_4, splitting it into H_2 and carbon. The outlet of the reactor is connected to the gas chromatograph (GC) for qualitative and quantitative analysis of gas compositions. The produced solid carbon will be deposited on the inner electrode bar and collected after the reaction.

4.2.2 Construction and validating the operation of plasma reactor and plasma-based test system

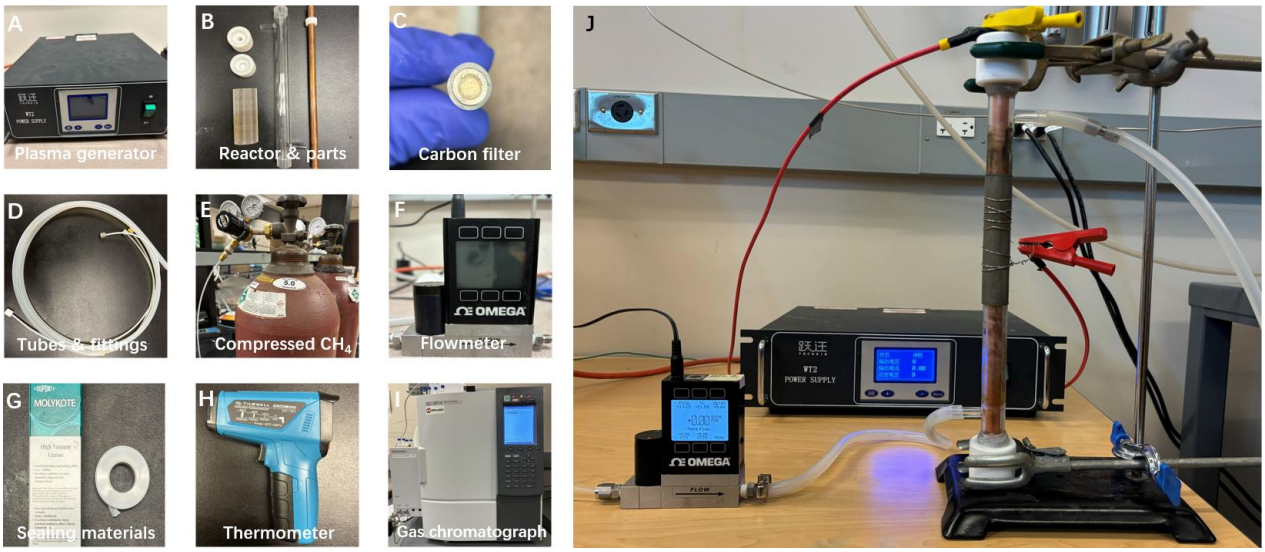

Fig. 4.2-2. Photographs of main components, parts and instruments for constructing the plasma reactor and the test system (A-I); a close-up view of the as-constructed plasma reactor connected with the gas flowmeter and the plasma generator (J).

Main components, parts and instruments for the assembly of the plasma-based test system is shown in Fig. 4.2-2A-I, including the plasma generator, the plasma reactor tube and electrodes, solid carbon filter, gas pipes and fittings, CH_4 cylinder, gas flowmeter, Teflon tape and vacuum silicone grease, thermometer, and gas chromatograph. These elements will be connected and constructed to a whole plasma-based test system as designed in Section 4.2.1.

A close-up view of the as-constructed plasma reactor connected with the gas flowmeter and the plasma generator is shown in Fig. 4.2-2J. At upstream, the reactor is connected with CH_4 cylinder via the gas flowmeter. At downstream, the plasma reactor is connected to GC for performance characterizations. The two electrodes of the plasma reactor are connected to the plasma generator by wires with red and yellow clamps.

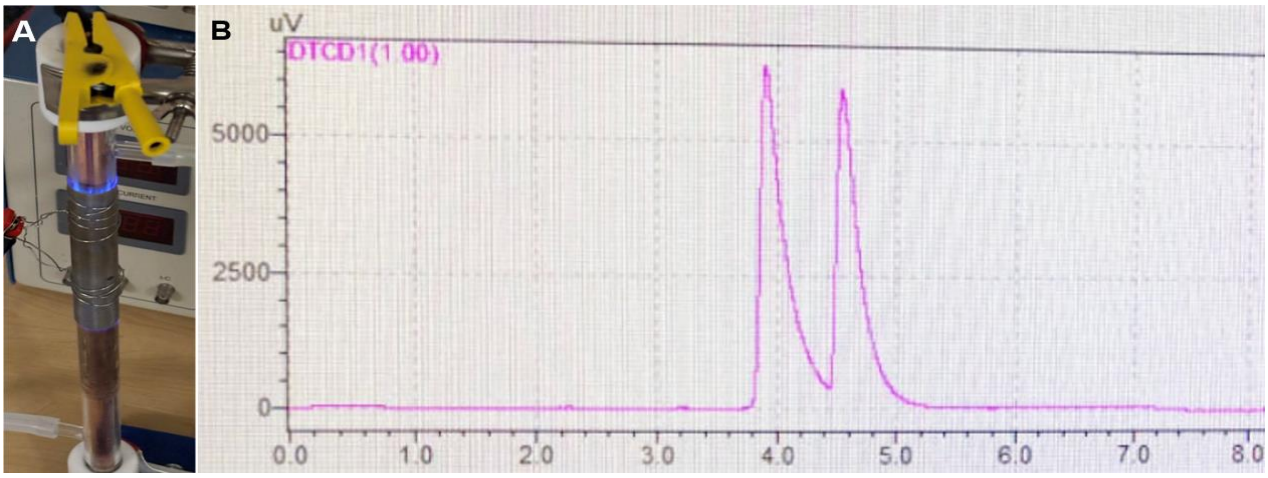

Fig. 4.2-3. (A) Photograph of the plasma reactor during operation, where the purple light of the plasma can be observed. (B) Real-time screenshot of the online collected gas composition in GC from the outlet of the plasma reactor, showing the peaks of produced H_2 (left) and unreacted CH_4 (right).

The stable operation of the as-designed plasma reactor was demonstrated in Fig. 4.2-3A, where the purple light of the produced plasma state can be observed clearly. When the CH_4 gas flowed through the plasma region, the splitting of CH_4 occurred. The production of H_2 from CH_4 splitting was further demonstrated by observing the H_2 peak in the GC spectrum (the left peak in Fig. 4.2-3B). These results validated the successful operation of the plasma reactor and the plasma-based test system.

4.2.3 Evaluation of CH_4 conversion and energy consumption

The measured GC peaks areas of H_2 and CH_4 were calibrated by standard gases with various H_2/CH_4 ratios to obtain their concentrations at the reactor outlet. Furthermore, the total gas flowrate at the outlet of the plasma reactor (including produced H_2 and unreacted CH_4) was recorded during the reaction. Thus, the respective flowrates of H_2 and CH_4 at the reactor outlet can be derived. Then, the actual amounts (moles) of H_2 and CH_4 collected during a certain time duration can be calculated based on the recorded time on stream.

The conversion of CH_4 was defined as the following:

$$CH_4 \text{ conversion } (\%) = (\text{amount of } CH_4 \text{ consumed}) / (\text{amount of } CH_4 \text{ input}) \times 100\%$$

The energy consumption of the reaction was evaluated by the following equation:

$$\text{Energy consumption } (kWh/kg\ H_2) = \text{Electricity consumed} / \text{amount of } H_2 \text{ produced}$$

where the electricity consumed (power) was calculated by the product of the measured current through the reactor and the voltage applied to the reactor.

4.3 Subproject 1: PV-AEM electrolyzer integration for Green Hydrogen

4.3.1 PV System 1: Design of Off grid PV and DC-DC converter with battery-based model for small 3 cell version of AEM electrolyzer and photobioreactor

1. Design parameters:

- System voltage:12V
- PV: 400W
- Battery: 2, 12V,50Ah battery
- Converter: CC-CV supply (0-12V, 0-20A)
- Optimal operation of AEM: 6V, 12A (72W)
- DC pump: 12V, 4A (max)
- MPPT specification: 30A
- Inverter for photobioreactor: 120V, 300W

2. Schematic designs of integrated system:

Figure. 4.3.1 below describes a schematic of the integrated system.

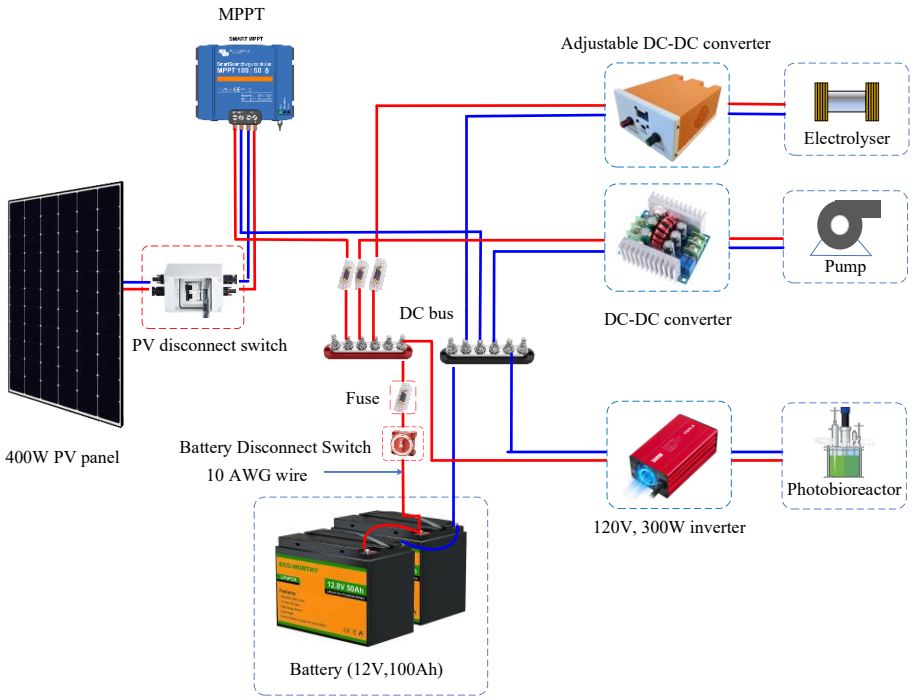

Figure 4.3.1. Schematic diagram of the integrated system

3. AEM specification:

Cipher Neutron supplied a small AEM electrolyzer and a 5 kW electrolyzer. The small electrolyzer is supplied by Cipher neutron has the following specifications:

- Number of cells: 3
- Operating voltage: 0-6.6V
- Cell area: 50cm2
- Current range: 0-50A

Figure 4.3.2 shows a photograph of the electrolyzer and figure 4.3.3 shows the PCB and 3D encloser of the converter.

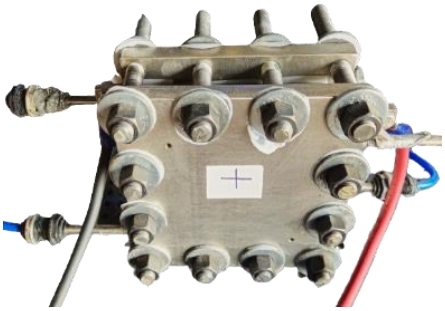

Fig.4.3. 2 The AEM Electrolyzer cell

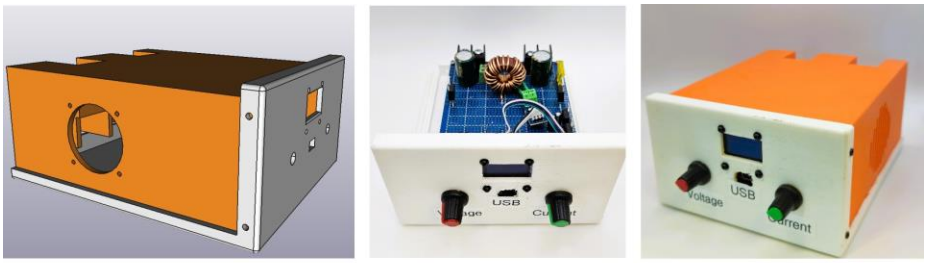

(a) (b) (c)

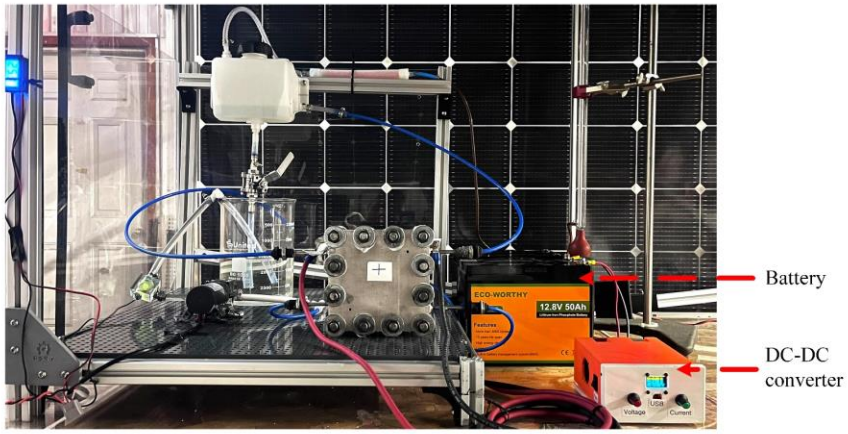

(d)

Figure 4.3.3. (a) 3-D encloser design; (b) PCB design of DC-DC converter; (c) Assembly of the converter; (d) Final off grid PV supply setup for AEM electrolyzer.

After design and construction, integration was performed with the plasma reactor, AEM electrolyzer and the bench scale photobioreactor. These are shown below:

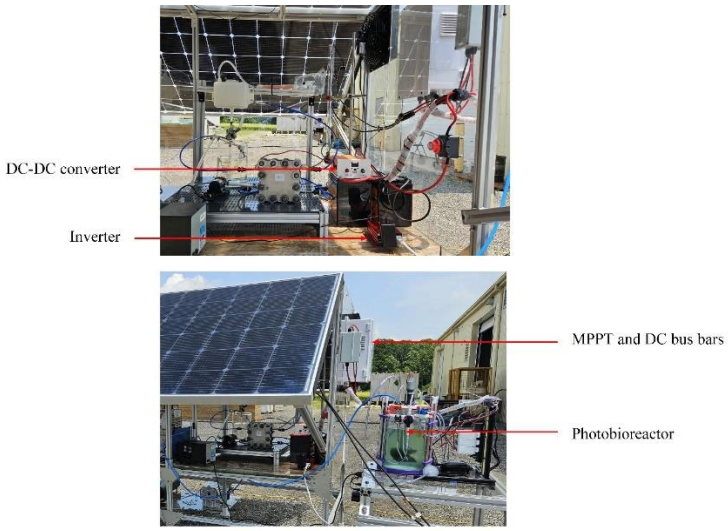

Fig. 4.3.4. Small AEM and photobioreactor setup

4.3.2 System 2: Design of Off grid PV and DC-DC converter with battery-based model for a smal 3 cell version of AEM electrolyzer and photobioreactor

The Low-Temperature Plasma Experimental Power Supply (WT2) was a 1kW DC magnetron puttering plating power supply operates at 230V (50Hz) with an output range of 0-30kV and 0-500W and is suitable for various gas reactors. 400W silicon-based PV modules were used. The system used two LiFePO4 12V, 50Ah batteries, connected in series, to provide a 24-hour backup power supply at 24V DC. A 24V, 20A MPPT wasemployed for optimal PV performance and battery charging. An inverter, designed with the EGS002 driver and rated at 175W AC, converts the 24V DC to 230V AC to meet the power requirements of the WT2 power supply. The inverter includes a feedback loop to maintain a stable 230V AC output. These are illustrated in the photographs below.

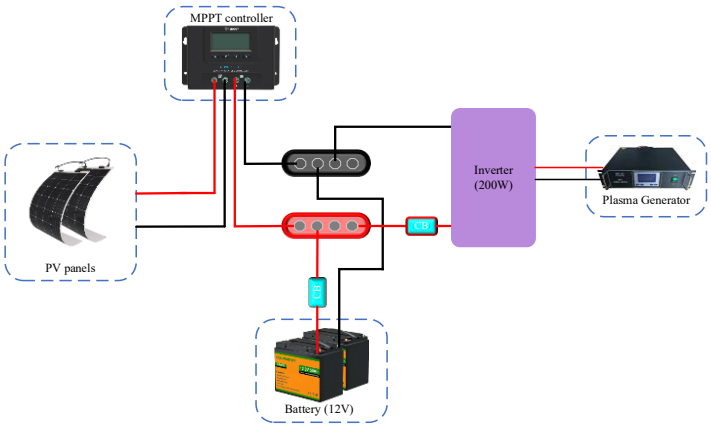

Fig. 4.3.5. Block diagram of portable solar-powered plasma generation system.

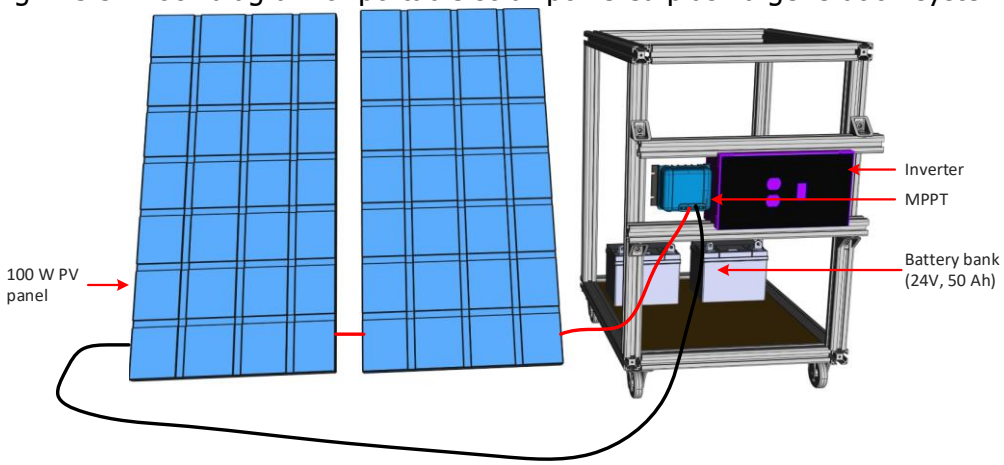

Fig. 4.3.6. Complete model of portable solar power supply for plasma generator.

Design procedure:

Inverter design: An open-source Inverter was designed and its design file and bill of materials and other instruction are fully open source. The populated PCB and interconnections are shown below.

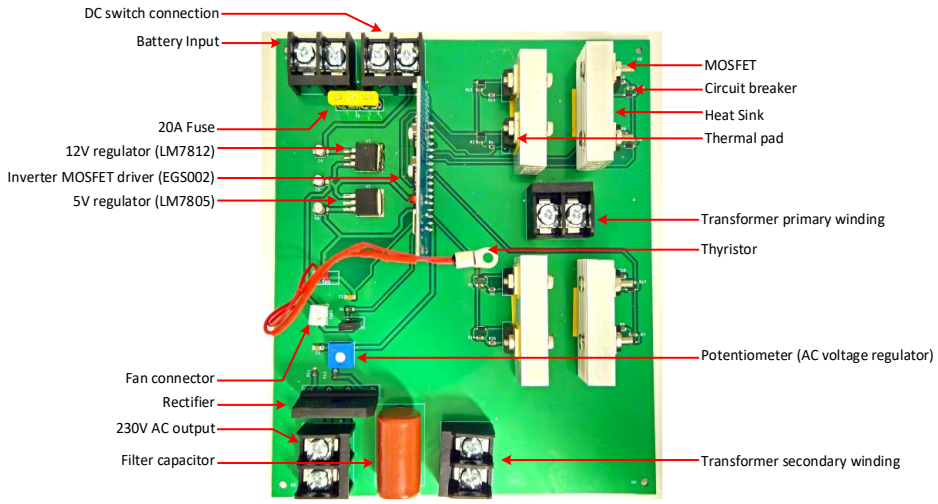

Fig. 4.3.7. Populated PCB and transformer interconnection.

Encloser design: An encloser was built as per the figure below. A portable trolley was also assembled for this purpose and is also depicted below.

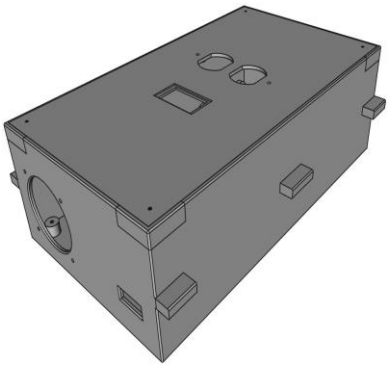

Fig. 4.3.8. Inverter encloser.

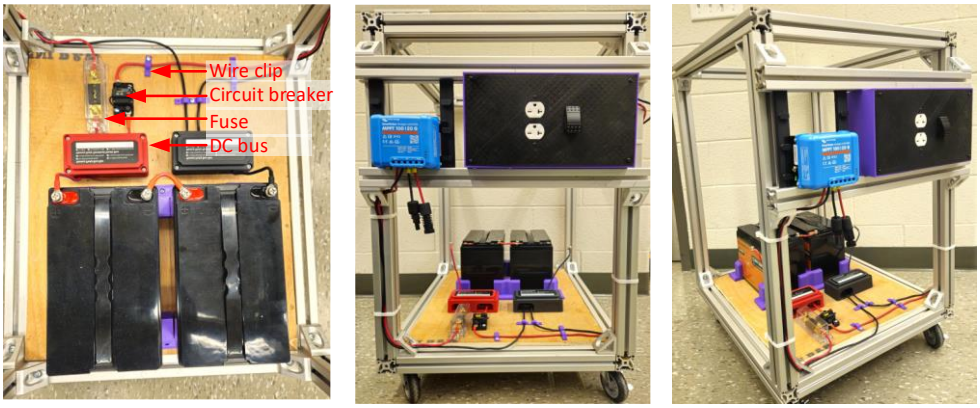

(a) (b) (c)

Fig. 4.3.9. (a) Battery and protection equipment connections (b), (c) Full setup view.

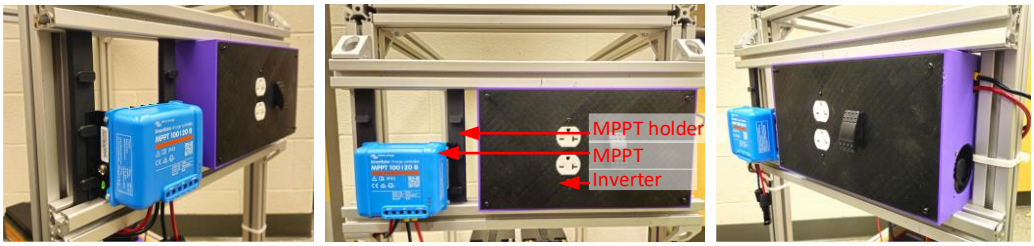

(a) (b) (c)

Fig. 4.3.10. MPPT and Inverter installation (a) left, (b) center and (c) right sides.
Testing with open-source inverter and portable trolley

The assembled test system is shown below.

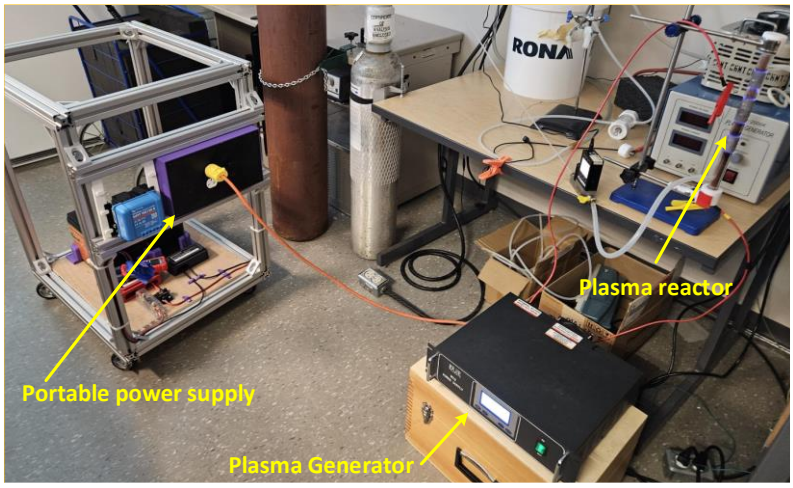

Fig. 4.3.11. Assembled plasma test system with portable power supply.

Final demonstration of small-scale integrated pale blue hydrogen production system

The PV box, designed to operate outdoors, was 1.8 meter tall and 2 meter long, standing on 6 legs and able to hold up to 1050 lb. of weight. At the bottom the 6 wheels made it able to be moved and placed anywhere easily in any type of terrain. The structure was made of aluminum extrusion 3030 as shown below. It had 3 solar panels of 2 meter by 1 meter which had the capacity of 400 W each. On the remaining sides, the box presented 2 opening polycarbonate

panels on one side, to have an easy access inside without lifting the panels and a 12-inch fan on the other side which guarantees 0.3 m^3 /s of airflow to ventilate the inside of the box.

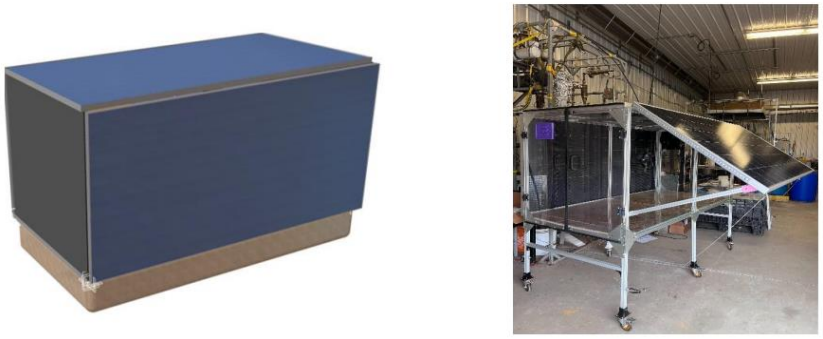

A B

Figure 4.3.12: PV box A) 3D design; B) Realization

The panels of the box, placed on the sides were able to be lifted and rotated. According to the data from NREL the optimum angle for London, Ontario is 34° to maximize the production from the solar panels. In order to do so 2 different designs were created to hold the panel in the right angle as shown in Figure 4.3.13. The design of these pieces considered the necessity to be able to easily open and close the solar panels according to the needs. The wind load has been taken into consideration by adding 2 aluminum cables (4 mm thick) which go from the structure to the panels once opened, to avoid them to flip during windy days.

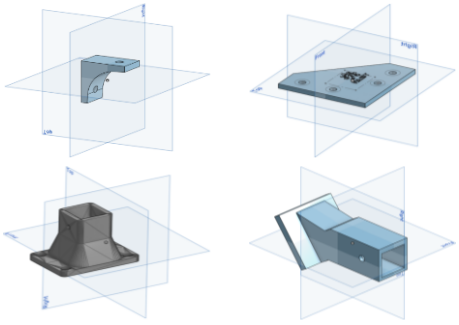

Figure 4.3.13: Polycarbonate PV box supports

To be able to work outside the box, the box has been tested following the Ingress Protection (IP) standards for water and dust. Considering the box with panels down, like in the figure above, , the IP rating is IP54 and we are currently working to make it IP55.


Figure 4.3.14: PV box closed

Ratings for Ingress by Dust			
IP5X	Dust protected	Tested by inspection to ensure any dust that enters would not interfere with the part's functionality	✓
IP6X	Dust tight	No ingress of dust at all	✗
Ratings for Ingress of Water			
IPX0	No protection	Item not protected at all against ingress of water	
IPX1	Vertical protection	Item protected against vertically falling water droplets, no damage or interruption of functions of components	✓
IPX2	15° Protection	Rating extends IPX1 by ensuring protection against falling water droplets at the angle up to 15 degrees from vertical	✓
IPX3	60° Protection	Safe from ingress of water sprayed up to 60 degrees from vertical impact	✓
IPX4	Any direction	Extends IPX3 including water splashing from any directions. Tested for at least 10 mins with no harmful effects	✓
IPX5	Low-pressure jet	Item protected against from low-pressure water jets directed from any angle with limited ingress with no harmful effects	✗
IPX6	1-Bar water jet	This rating extends IPX5, with a water pressure reaching up to 1 bar	✗

Finally, the complete setup is shown in Figure 4.3.15. , as highlighted, on the left has been placed the plasma generator with 2 gas cylinders, on the right the 3-cell AEM has been placed with its setup for drying and collecting gas next to battery pack, DC-DC convert. Outside the box has been placed the MPPT and electrical connections inside an electrical enclosure and on the cart the photobioreactor with his own MPPT and electrical connections.

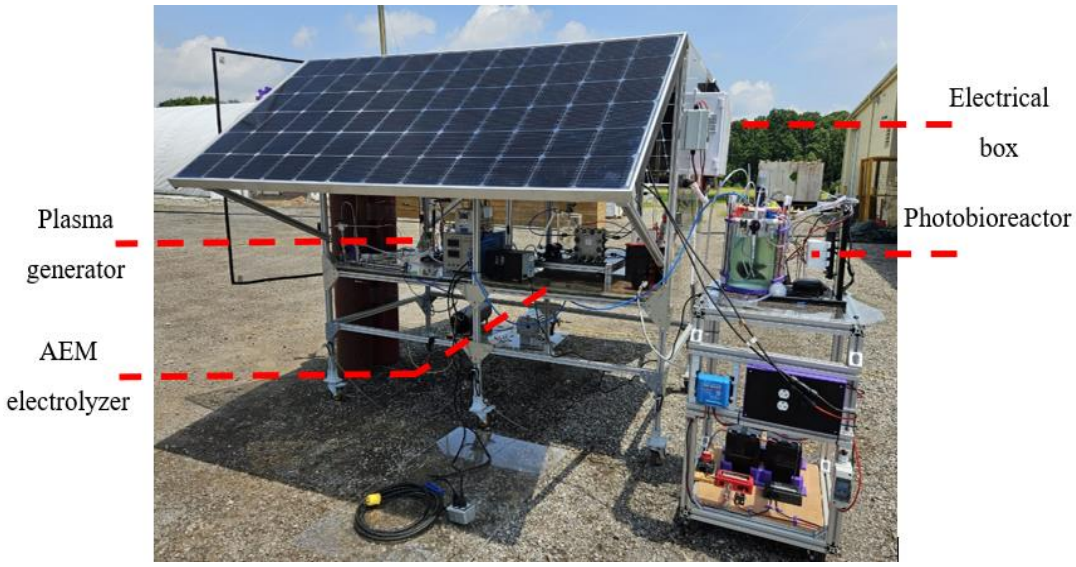

Figure 4.3.15 Final setup PV box

7kW FPV and 5kW AEM Specifications and Power Supply Design: Summary of Activities Performed in Medium-Scale PV and AEM Sub-Project

The primary responsibility of this subproject is to integrate and validate solar photovoltaic (PV) systems for demonstration purposes. Additionally, the project involves testing Cipher Neutron's 5kW AEM electrolyzer and designing a power supply to ensure its proper functioning. Cipher Neutron has supplied the 5kW AEM electrolyzer for this project, which uses PV power to produce 82 grams of green hydrogen per hour (1000 liters/hour). The key activities performed on the large-scale PV system and the AEM electrolyzer are summarized below:

- **Selection of Project Site and PV System**: Choose an appropriate site and determine the type of PV system to be used.
- **Design and Installation of Floatovoltaics**: Design and install a 7kW foam-based floating PV system (floatovoltaics) at the Western Innovation for Renewable Energy Deployment (WIRED), located at the Environmental Sciences Western (ESW) Field Station, an off-campus research facility of Western University.
- **Electrical Integration and Power Conditioning**: Develop an electrical enclosure and complete the necessary electrical wiring and power conditioning to create a generator capable of supplying the AEM electrolyzer. The power conditioning elements include charge controllers, inverters, and a battery bank.
- **Meteorological Data Collection**: Set up a meteorological station to collect local meteorological data, including ambient temperature, pressure, wind speed and direction, relative humidity, dew point temperature, precipitation patterns, and solar irradiation.

- **Installation and Configuration of the Electrolyzer**: Install and configure the 5kW commercial electrolyzer from Cipher Neutron.
- **System Demonstration**: Demonstrate the system's operation at the ESW Field Station.

Project Site Selection and Floating PV System Technology

Site Information: The Environmental Sciences Western (ESW) Field Station is an off-campus research facility located within the Faculty of Engineering at The University of ggggWestern Ontario. The ESW occupies a 33-hectare property that hosts the Biology Department's Field Station, the Institute for Chemical Fuels from Alternative Resources (ICFAR), as well as the Western Innovation for Renewable Energy Deployment (WIRED). The ESW primary mission is to spearhead the development of technologies and processes for producing chemicals and fuels from alternative resources, with a strong focus on green engineering and environmental sustainability. In terms of water surface, the facility consists of one large pond and eight man-made ponds. These ponds have been incorporated into the WIRED system to **test floatovoltaics**. The proposed plan involved harnessing the large pond's potential by deploying a floatovoltaic system on its surface to generate electricity for the large electrolyzer. Additionally, one of the small ponds was used as a photobioreactor.

Pond Specification (Figure 4.3.16): The large pond specifications are as follows: Length: 42m, Width: 35m, Total area: 1475m^2; Total potential floatovoltaic installation capacity: 250 kW (Approx).

Figure 4.3.16. (a) An aerial view of ICFAR. (b) Aerial zoom-in view of the large pond for FPV.
Floating PV or Floatovoltaics

Floating photovoltaics (FPV) are a recent advancement in PV technology that addresses the land use conflicts associated with large-scale PV installations. FPV systems exploit unused water surfaces and benefit from enhanced cooling from the water, reducing water evaporation and conserving water. The FPV modules developed by the Pearce group employed a foam-based floating structure, constructed with foam, marine sealant, and zip ties. Each module requires four pieces of polyethylene foam to ensure floatability, 281 grams of marine sealant, and 8.2 grams of zip ties for stability.

A 0.6 kW floating PV system was first tested on a smaller scale (Figure 4.3.175) in the man-made ponds at ICFAR to validate its operation in freezing conditions. The experimental phase demonstrated that circulating air in the water around the modules prevents ice formation and preserves the integrity of the PV modules. Consequently, FPV has been adopted for the large-scale PV system in this project.

Figure 4.3.17. Installed mini pilot floatovoltaic system at WIRED (In small human-made pond).
Design and Installation of 7kW foam-based FPV system

System Design: The 7kW FPV system was a scaled-up version of the previously installed 0.6kW experimental FPV. Initially, the FPV was designed to be 8kW but was reduced to 7kW due to geometric and practical engineering design constraints. The 7kW FPV system is composed of four different arrays, each connected to a separate Maximum Power Point Tracker (MPPT) for enhanced flexibility, modularity, and controllability. Each FPV array consists of two strings in parallel, with each string comprising five modules in series. This layout was chosen to facilitate the system's deployment on the water surface. :

Module Assembly Procedure: Each foam-based FPV module is modified after purchase and consists of three layers: a flexible PV module, an adhesive layer, and a foam layer. The foam is designed to ensure the module and all accessories float on the water surface. The assembly methodology for these modules has been developed by the FAST lab. First, the foam roll is cut into squares measuring 62.5 cm x 32 cm. Each module requires four foam squares to ensure the solar cells float at least 1.2 cm above the water surface. A semi-permanent, environmentally friendly marine adhesive is applied and spread on the back of the modules in four squares matching the dimensions of the foam squares. The foam squares are then bonded to the modules through pressure application. The assembled modules are kept under pressure for a minimum of 48 hours to ensure complete adhesion, after which the edges of the foam are sealed with an additional layer of adhesive. The foam used is closed-cell foam, which reduces the chances of delamination.

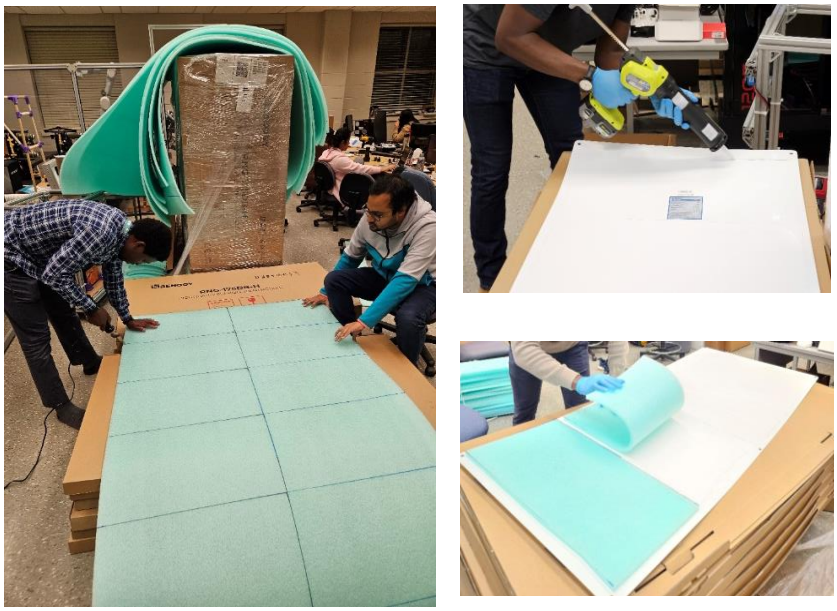

Figure 4.3.18. Assembly procedure of a foam-based floating PV module

Array Assembly Procedure : The array assembly begins with testing the individual assembled PV modules to ensure they all have the same range of open-circuit voltage (Voc) and short-circuit current (Isc). This is done using a multimeter and an open-source IV-curve tracer to characterize the modules. Once the modules are tested, they are connected in series and parallel configurations. After making the electrical connections, airlines are installed to supply air and prevent ice formation in the winter. The arrays are then deployed on the pond and anchored to the shore using metal poles buried 4 feet into the ground. This process is repeated for the remaining three arrays, providing a modular procedure for deploying foam-based FPV systems.

Figure 4.3.19. Assembled array before deployment.

PV System Deployment

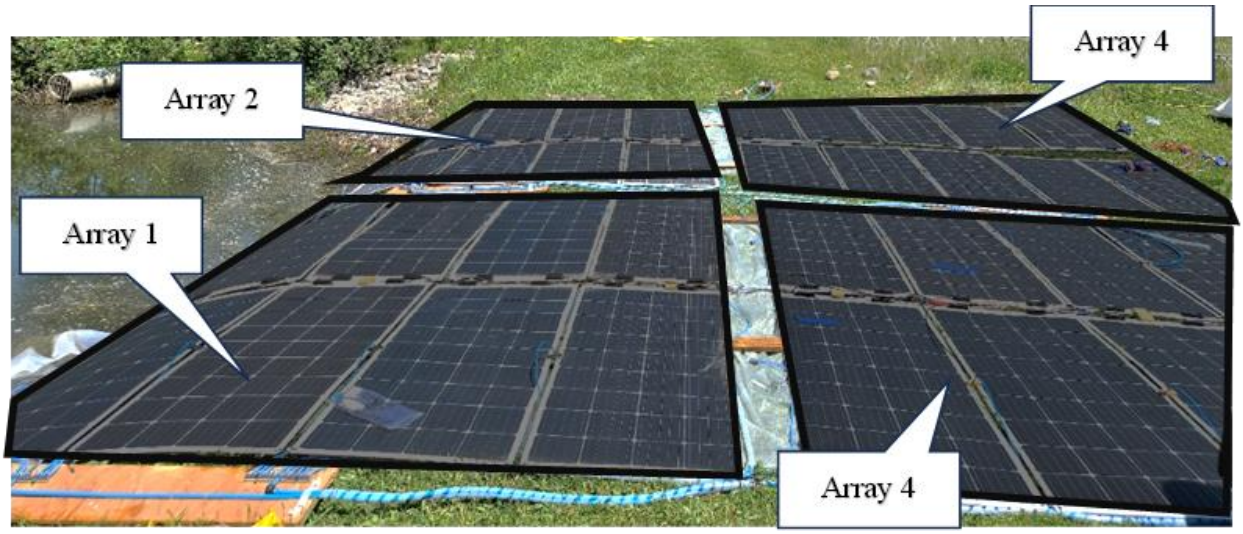

Figure 4.3.20 7kW foam-based FPV array on the shore before deployment.

The deployment of the 7kW PV system on the water occurred in four steps. First, the four assembled arrays were transported to the shore of the pond. Then, the system's electrical connections were wired, but the strings were not interconnected. Following this, the airline connections were made. Finally, the system was gradually pushed onto the water surface.

Figure 4.3.21 7kW FPV floating on the large pond at the ESW Field Station

The equipment required during the assembly and deployment of the FPV system are shown below.

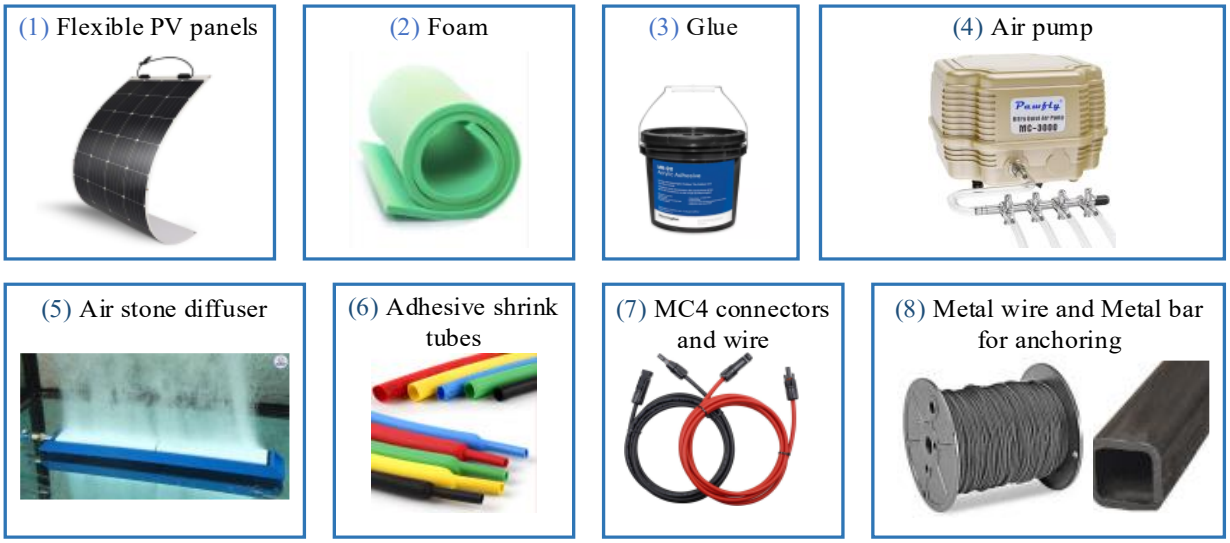

Figure 4.3.22. FPV system components.

Off-Grid Foam-Based FPV Power Supply: The PV power supply built from the 7kW FPV system is composed of three inverters. These three inverters are connected in parallel to supply the required voltage level for the AEM electrolyzer (3-phase, 400V line-to-line) with a total power capacity of 9kW. This 3-phase inverter-driven power supply is linked to the 7kW PV system through a set of four Maximum Power Point Tracking (MPPT) charge controllers, with each controller connected to one array of the FPV system. Additionally, a 10kWh battery storage system is integrated into the setup to provide stability and ensure the inverters operate properly, as the system operates completely off-grid.

The primary goal of the hydrogen plant is to provide an alternative outlet for excess energy generated by the PV system. PV systems often generate surplus energy during off-peak load situations, and employing an AEM hydrogen generator is an ideal way to utilize this excess energy. Therefore, the battery's purpose is not to ensure uninterrupted power supply to the electrolyzer but rather to stabilize power fluctuations specifically during daylight hours. The sizing of the PV system is determined based on the total load of the electrolyzer. In situations where sunlight is unavailable, the electrolyzer can be deactivated to optimize energy utilization.

Power Supply Specifications. The electrical specification of the power supply elements are as follows:

The electrical specification of the power supply elements are as follows:

- Solar Panels
  - Model: Renogy RNG-175DB-H-CA
  - Quantity: 40
  - DC Power: 175W/module (7kW in total)
  - Technology: multi-crystalline silicon
- 3-phase inverters bank

  - Model: Victron Energy MultiPlus-II 48/3000/35-32
  - Quantity: 3
  - Single Phase AC Voltage: 230V
  - DC Input Voltage 48V
  - Power: 3kW/ inverter (9kW in total)
  - 3-phase configurations Y-connected (230V/400V)
- MPPT Controllers:
  - Model:
  - Quantity: 4 (1 per PV array)
  - Maximum input voltage: 150V
  - Charging current: 35A
- Batteries:
  - Model: EG4 Electronics EG4 LL
  - Quantity: 2
  - Power: 5kWh/battery (10kWh in total)

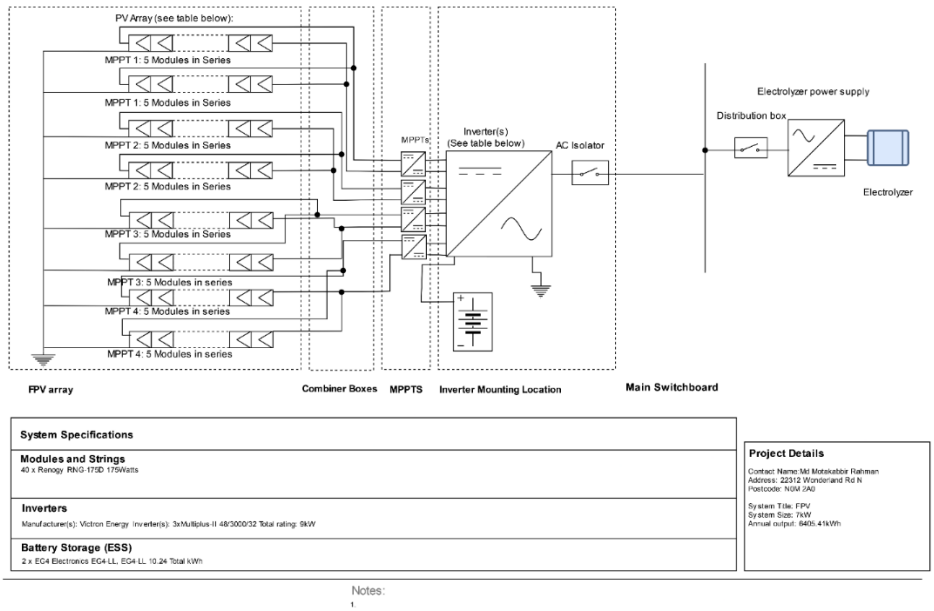

Figure 4.3.23. Single line diagram of the FPV power supply connected to the AEM electrolyzer

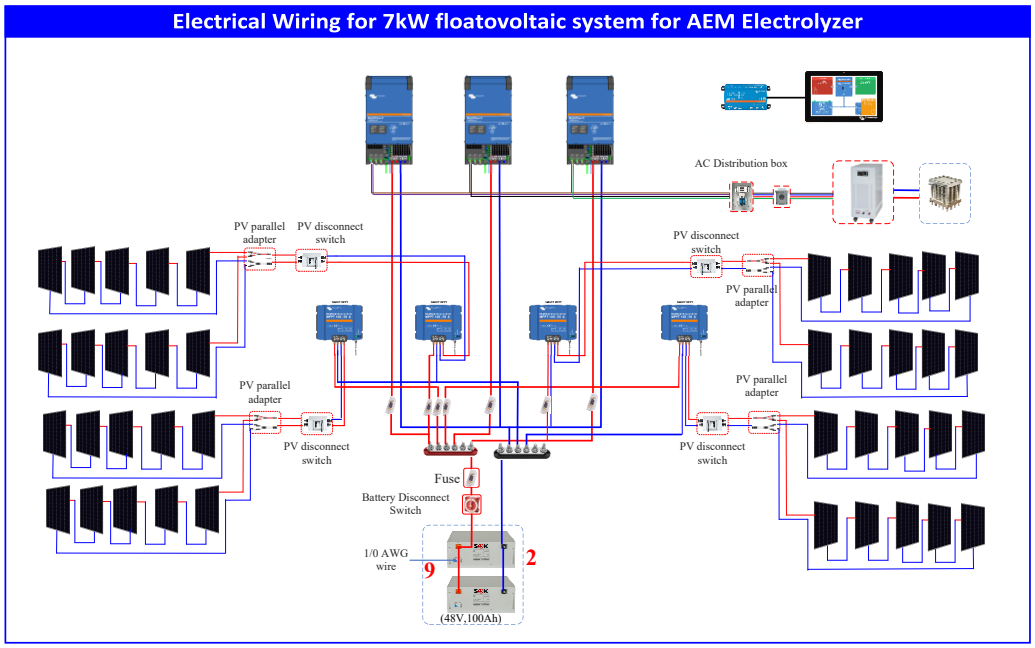

Figure 4.3.24. Electrical wiring diagram of the FPV power supply

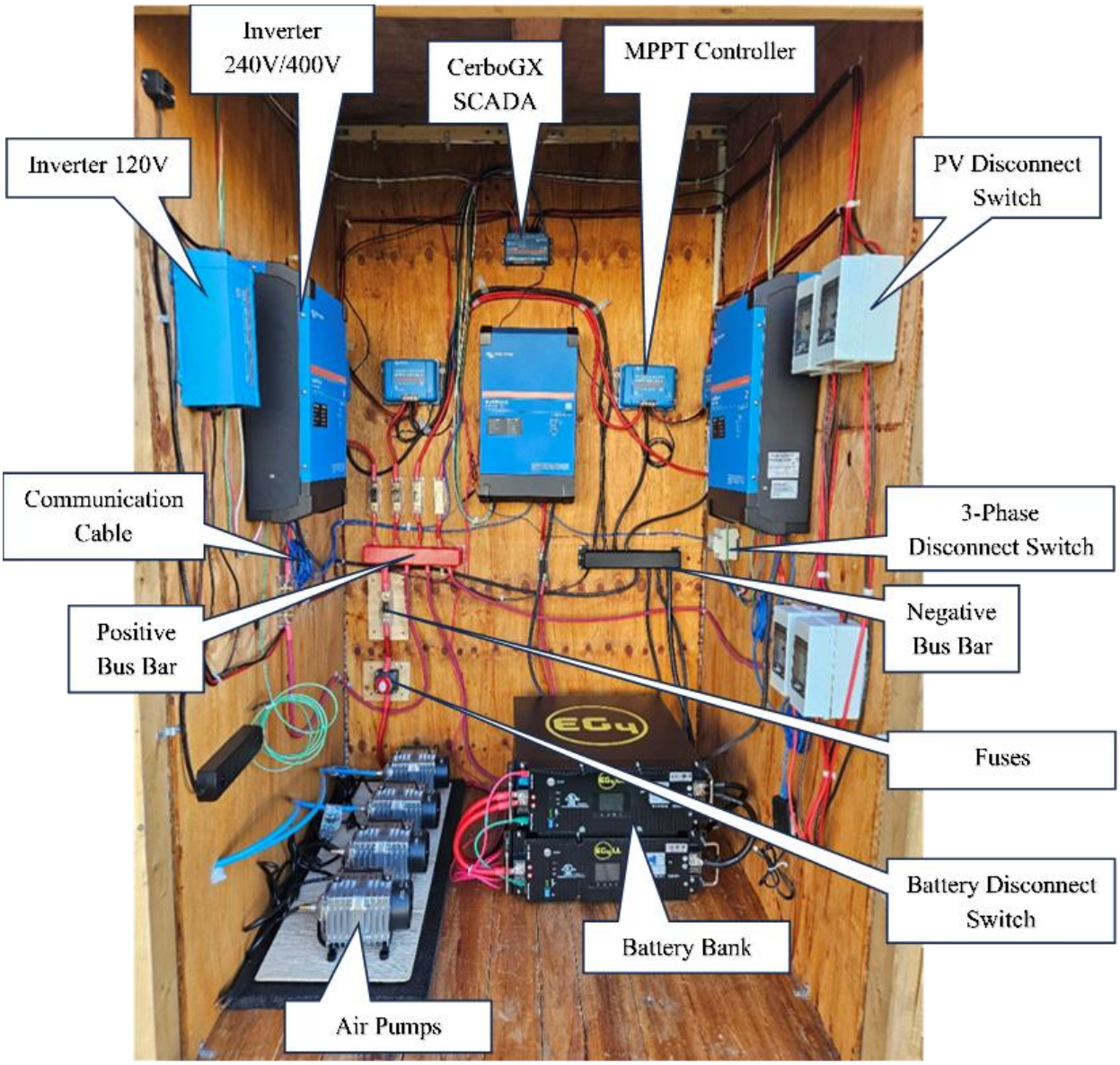

Figure 4.3.25 . Power supply electrical box with components label.

Data Collection: The data collection equipment for the system is split into 2 categories. The electrical data collection system is integrated with the chosen Victron MPPT controllers and inverters. This equipment can record the system's operating voltage and current both on the DC and the AC side. The controllers, inverters, and batteries are connected to a SCADA system from Victron Energy (CerboGX). The second data acquisition equipment is an open-source resistive datalogger that monitors air temperature, water temperature, and relative humidity, and collects infrared and visible light images of the system. This open-source equipment has been tested and

is ready to operated once Wi-Fi signal has been configured for the installation location. The solar irradiation and the wind speed are monitored by a MET station on site.

5kW AEM specifications:

- Total Cells: 27
- Voltage Range per Cell: 1.8 to 2 Volts
- Operating Amperage: 100 Amps
- Maximum Amperage: 250 Amps
- Operating Voltage: 47.3 Volts

- Maximum Voltage: 52 Volts
- Hydrogen Production at 5 kW: 1,000 liters/hour
- Electrolyte: 1M KOH
- Hydrogen Production at 5 kW: 1,000 liters/hour (89g/hr)
- Production Rate: 200 liters/kWh

AEM AC/DC power supply specifications:

- Input voltage: Example: 400V, 3phase
- Max output: 0-50V, 0-200A
- Power supply's plug name: NEMA 17-30P

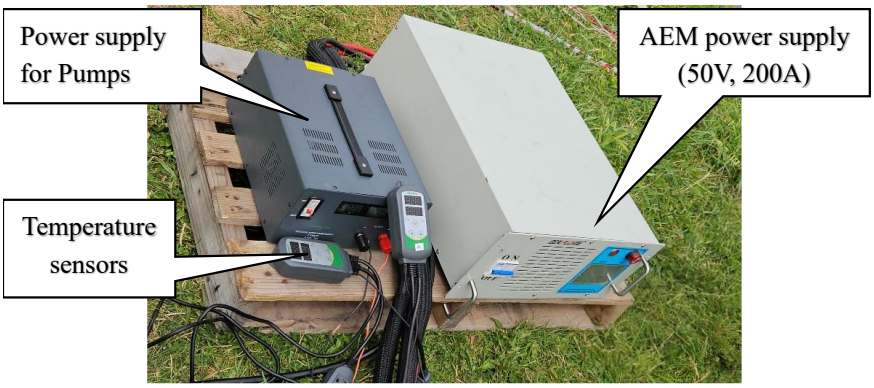

Figure 4.3.26 AC/DC power supply for5 kW AEM and Pump

Complete System Operation During Integration and Demonsration

During the integration and demonstration, the AEM electrolyzer was operated and powered by a fully off-grid foam-based FPV system. The hydrogen generator demonstrated resilience to fluctuations from the PV system, maintaining continuous operation despite changes in weather from clear skies to cloudy conditions. The power required by the AEM was primarily supplied by the PV system, with any additional power needed supplied by the battery. For instance, in the scenario depicted in Figure 4.3.25, the AEM was drawing 3.84 kW of power. Of this total, 2.52 kW was supplied directly from the PV system, while the battery contributed an additional 1.84

kW. The total power supplied exceeded the AEM's consumption because the 110V inverter powering the AEM pumps (0.53 kW) was not displayed on the CerboGX screen.

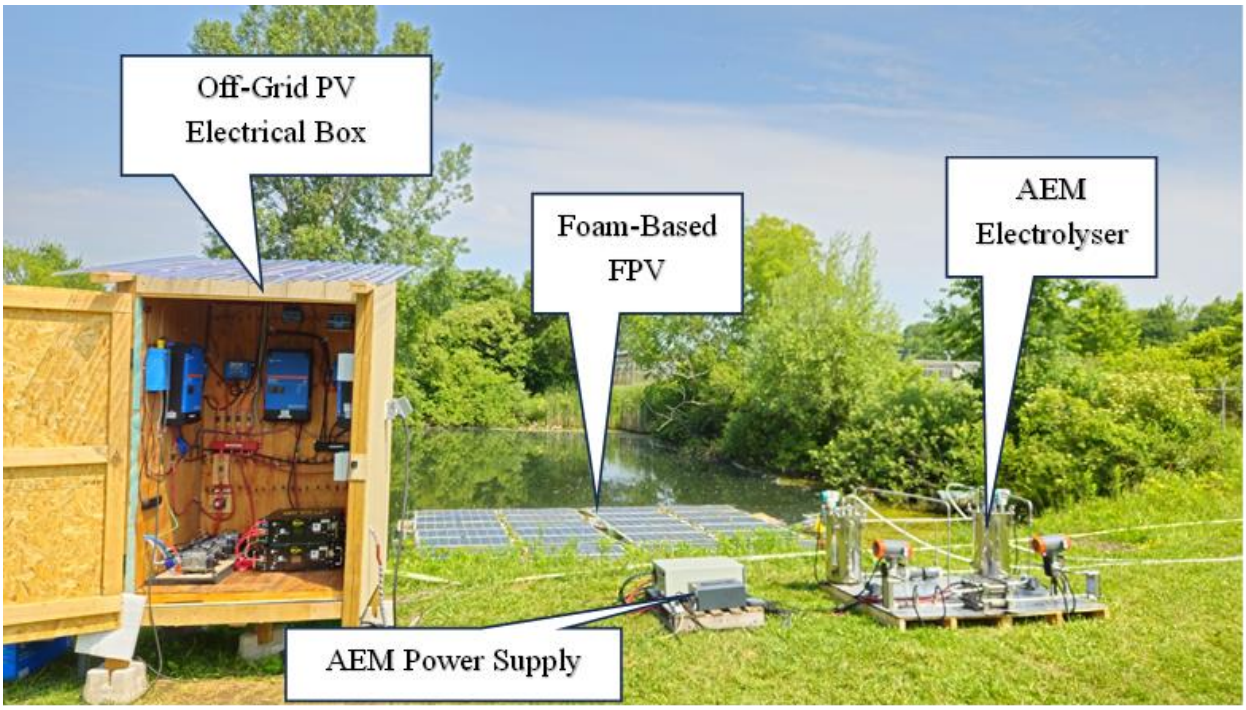

Figure 4.3.27. Complete system setup

4.4 Sub project 4: **Carbon capture and water recycle using a 500 L and a 20,000 L Photobioreactor.**

Goals: Microalgae *Chlorella vulgaris* were cultivated in a a 500 L and a 20000 L photobioreactor Clean water is recycled and the microalgae are converted to bioplastic for carbon capture

Growth media used for microalgal cultivation: *Chlorella vulgaris* **UTEX 2714** was used for this activity. For cell maintenance, the microalgae were routinely cultured on Bold's modified media (0.25 g.L^{-1} $NaNO_3$, 0.025 g.L^{-1} $CaCl_2.2H_2O$, 0.075 g.L^{-1} $MgSO_4.7H_2O$, 0.075 g.L^{-1} K_2HPO_4, 0.175 g.L^{-1} KH_2PO_4, 0.025 g .L^{-1} NaCl, 63.9 mg.L^{-1} Na_2EDTA, 4.98 mg L^{-1} $FeSO_4.7H_2O$, 11.42 mg .L^{-1} H_3BO_3, 8.82 mg.L^{-1} $ZnSO_4.7H_2O$, 1.44 mg .L^{-1} MnCl, 1.57 mg.L^{-1} $CuSO_4.5H_2O$). The pH of the BBM media was 6.6 and it sterilized in at 120^{o}C and 20 psig for 15 min.

For cultivation in 250 mL, 1 L flasks and 7 L and 15 L photo-bioreactors, the microalgae cultures were incubated at 20-25^o C with continuous air bubbling (ca. 7 L per min). The growth in 7 L photobioreactors, 500 L and 20,000 L photo-bioreactor was carried out using two different growth media, i.e., a simulated waste water containing MiracleGro^{TM} fertilizer or a second growth media consisting of insect frass waste at upto 10 g/L. The experimental set-up for the 500 L photobioreactors is shown in Figure 4.4.1 below.

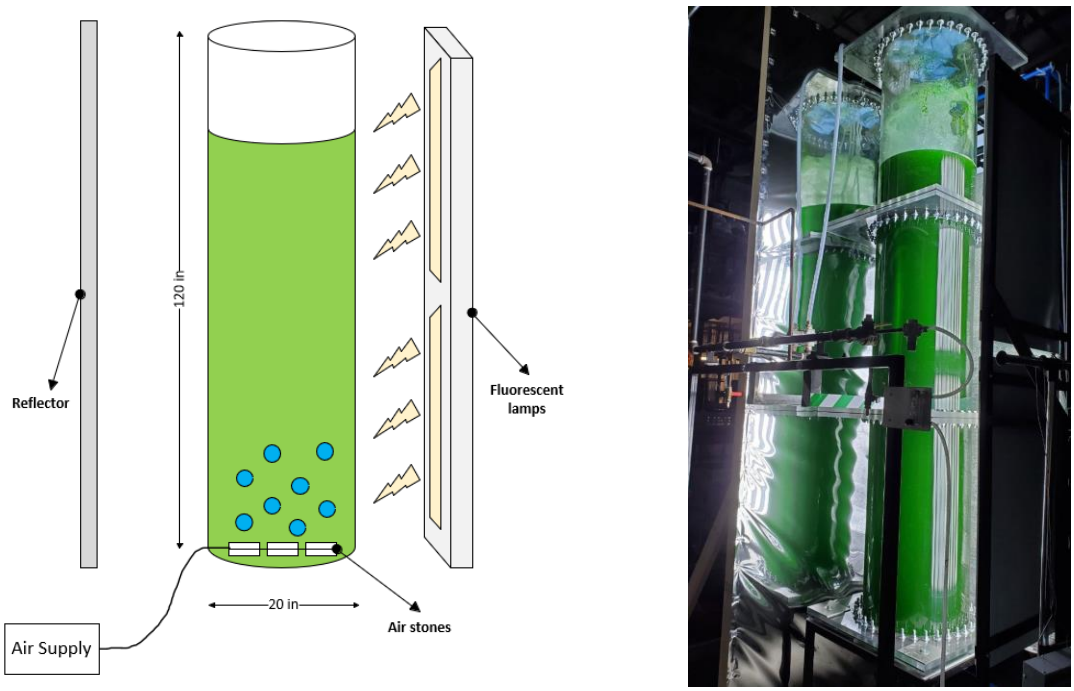

Fig. 4.4.1 500 L working volume photobioreactor for Chlorella cultivation

Microalgal biomass was measured using optical density at 686 nm using a spectrophotometer (Cary50-bio UV-visible; Varian, Palo Alto, CA). Cells were also counted using a hemocytometer.nitrogen content of the media and reactive phosphorus was measured using the a standard Hach kit with the appropriate range (HACH Loveland, CO).

Cell cultivation was carried out using 10 percent inoculum (e.g. 50 L in 500 L system) in each bioreactor utilized. Air was supplied though diffusers with the provision of adding generated CO_2 produced sub project 1. In the integration and demonstration the carbon dioxide was bubbled into a 14 L bench top bioreactor.

Open Source Photobioreactor Control)

The open-source photobioreactor, shown in Figure 4.4.2, was applied in the test demonstration. This photobioreactor has additional LED lights fixed around the growing vessel to support the photosynthesis for the microalgae. To monitor critical growth parameters in real time, a pH sensor, dissolved oxygen sensor, and temperature probe were included inside the vessel. In addition, a peristaltic pump was used to extract samples from the reactor to a turbidity sensor to monitor the biomass density. By calibrating the turbidity sensor beforehand with known biomass concentrations, real-time growth-rates could be monitored.

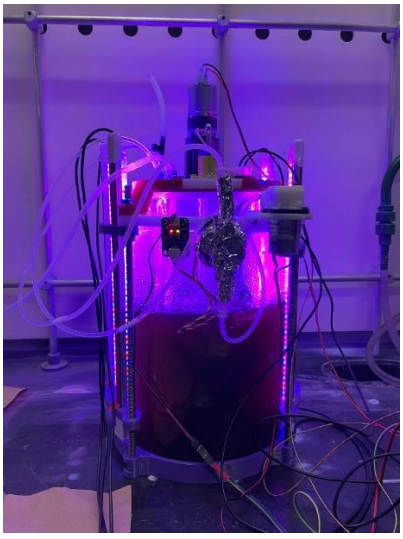

Figure 4.4.2: Photobioreactor used in the onsite test demonstration to bubble CO_2 generated from Sub project 1.

Growth in a 20,000 L pond bioreactor

A pond bioreactor system was constructed from an existing pond available at the ICFAr, Western University site . Please see Figure 4.4.3 below. The feed to the photobioreactor was a wastewater (fertilizer) stream containing nutrients (nitrogen and phosphorus). The pond has a diameter of 5 meters and a depth of 1 meter, with a capacity of approximately 20,000 liters of water. A water proof lining was installed at the base and around the perimeter walls. The pond system was fully functional with the installation of an air bubbler and air diffusers.

Pond.MP4

Video clip of 20000 L microalgal pond.

Figure. 4.4.3: Pond photobioreactor for on site microalgal cultivation

Solar Panel Specification:

The specifications of solar panel that is used for this purpose are given by the following table.

Table 2: Specification of solar panel

Manufactured by	HELIENE
Model no.	72M-320
Maximum Power (W)	320
Voltage MPP (V)	37.43
Current MPP (A)	8.55
Length (cm)	196
Width (cm)	99.6

Water recycling and cell concentration in the 500 L photobioreactor: The 500 L working volume photobioreactor is installed in the pilot plant in the Bassi lab at Western. This was used to demonstrate cell harvesting and water recycling as the indoor environment provided more controlled conditions. Figure 4.4.4 shows he set up for cell concentration and water recycling,

Figure 4.4.4: Photograph of the 500 L bioreactor with the ultrafiltration cell harvesting system

The biomass was obtained at the end of the cultivation (14 days) and was d harvested through ultrafiltration, centrifugation or gravitational settling agent. The figure above shows an ultrafiltration membrane which retains the microalgae and allows clean water to go throught. Smaller scale samples were concentrated using centrifugation. Centrifugation occurred at 10800rmp for 20 minutes using a SORVALL WX Ultra Series centrifuge (Thermo Electron Corporation). The clean water obtained was tested for possible use in the AEM electrolyzer during the integration step.

Carbon sequestration by converting to Eco-plastic. Carbon dioxide is taken by the microalgae at the rate of 1.8 Kg per Kg of biomass. The algae were converted to eco plastic and this enable the removal of carbon from the gas phase. Thus algae biomass is converted to bioplastic for carbon sequestration. The bioplastic composites were prepared as follows. Control samples were divided in two portions. Blend A with a composition of 20%, 65% and 15% of

glycerol, microalgae and pectin, respectively, and Blend B with a composition of 20%, 50%, and 30% of glycerol, microalgae and pectin, and crushed pine needle powder respectively. The blends were mixed at 60ºC using and hot plate magnetic stirrer for 30 minutes. Samples were pressed into molds of various shapes depending on desired testing before being placed in a muffle furnace (Thermo Fisher Scientific) and dried for 24 hours at 60ºC. Once dried, the solid bio-composite could be peeled from the mold and stored at room temperature. All samples were prepared using this method unless otherwise stated. Sample to be prepared for tensile testing were pressed flat into aluminum plates before being placed in the furnace to dry. Once dried, the solid disk could be peeled from the plate cut into strips with 5.0 x 0.5 x 0.2 cm dimensions. For compression samples, after mixing the bio-composite, the paste was placed in a plastic cylindrical tubing mold with the dimensions of 1.5 cm height and 0.5 cm diameter, then left to dry for 24 hours in the furnace at 60 ºC. Figure 4.4.5 shows the eco-plastic material prepared from the microalgae.
The bioplastic produced is shown in figure 4.4.4 below.

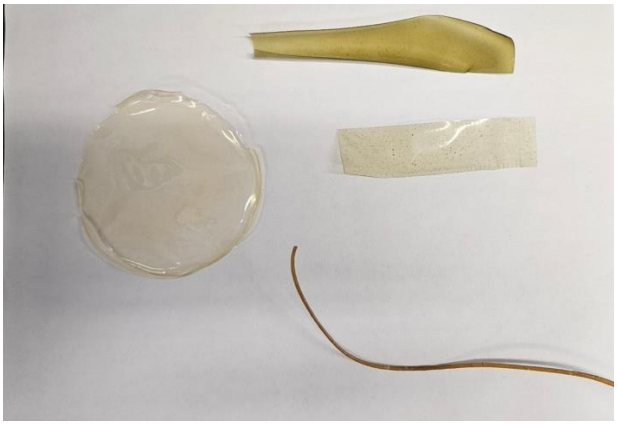

Figure 4.4.5: Different shapes of bioplastics made from microalgae cultivated in the 500 L bioreactor are shown.

5 Results and Analysis

5.1 Subproject 1: membrane separation

Membrane performance was assessed by measuring gas permeance and selectivity. Membrane fabrication process development was guided by these measurements. The performance was compared to commercial polymer gas separation modules and the most suitable membrane module for the demonstration system was selected. Membrane modules were then integrated in a demonstration unit to separate biogas upstream of the plasma reactor to deliver high purity methane to the plasma system and divert carbon dioxide to the photobioreactor for sequestration. A second membrane unit was installed downstream of the plasma reactor to extract product hydrogen and recycle unreacted methane through the plasma reactor to improve overall yield.

5.1.1 Permeance cell validation and commercial membrane baseline

Commercial membranes for biogas separation were acquired for the purpose of validating the cross-flow gas separation system and to compare to the achievable graphene membrane performance to decide which option will work best in the demonstration system. Figs. 5.1-1 and 5.1-2 show the measured membrane performance for biogas separation. At an applied transmembrane pressure difference of 40 psi, the membrane removes >99% of carbon dioxide resulting in good methane purity for downstream processing. This provides highly effective biogas separation and meets the purity requirements of the plasma system. Furthermore, this membrane unit was tested to flow rates of up to 200 sccm, more than sufficient to meet the requirements of the plasma system. The hollow fiber membranes currently perform best and were selected for the demonstration unit.

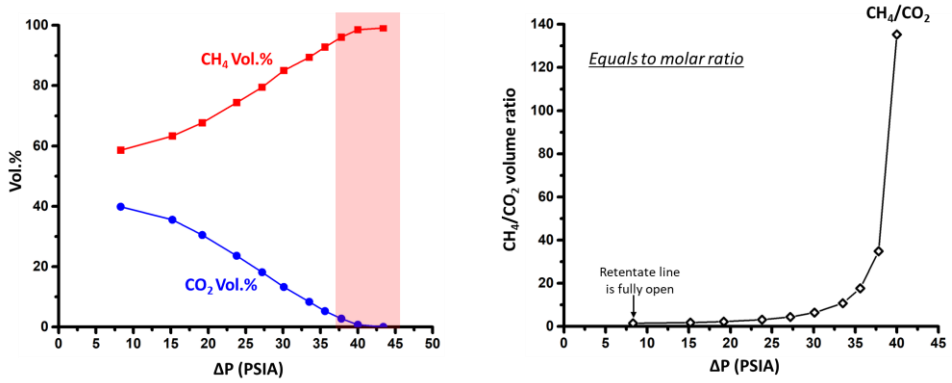

Fig. 5.1-1. Measured performance of hollow-fiber type biogas separation membrane. (left) Gas composition on retentate side vs pressure difference applied across membrane. (right) Ratio of carbon dioxide to methane on retentate side vs applied pressure difference.

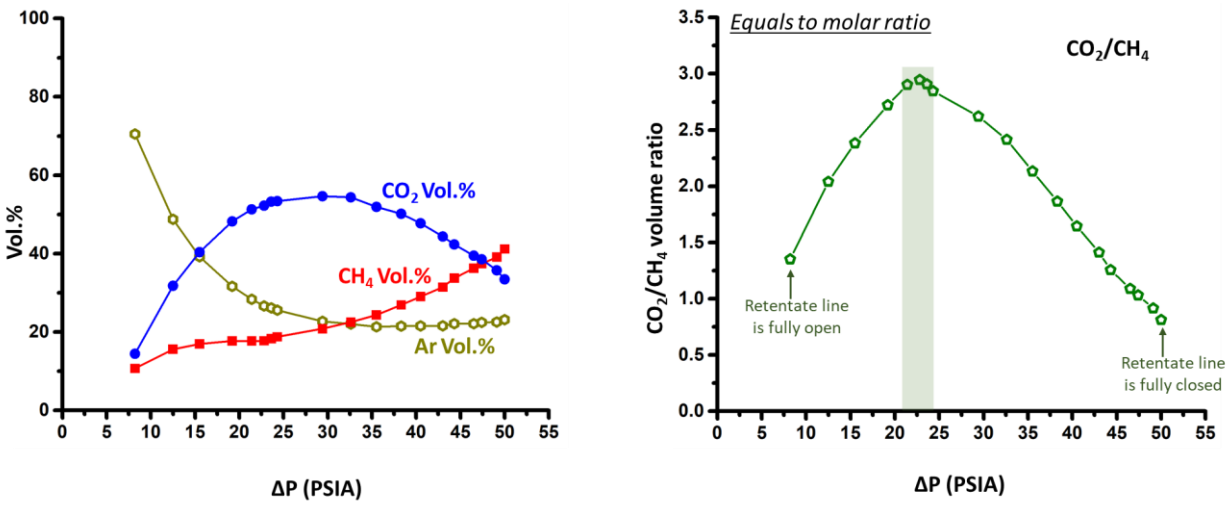

Fig. 5.1-2. Measured performance of hollow-fiber type biogas separation membrane. (left) Gas composition on permeate side vs pressure difference applied across membrane. (right) Ratio of carbon dioxide to methane on permeate side vs applied pressure difference.

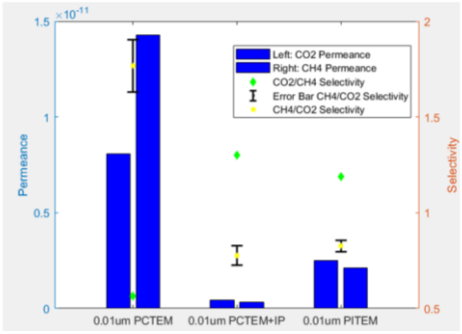

Fig. 5.1-3. Initial graphene membrane permeance and selectivity measurements.

5.1.2 Graphene material quality and membrane comparison

The original project scope included the possibility of upgrading existing chemical vapor deposition system hardware for graphene growth and using it to produce graphene for the project, if it was determined to be needed to achieve the required graphene quality or to produce the required areas of graphene. During membrane design and fabrication, it was found that the quality and price of commercially available graphene was suitable for the project and these upgrades were not necessary. Furthermore, it was found that the conversion rate of the non-thermal plasma process could be increased by separating hydrogen downstream and recycling unreacted methane through the plasma chamber. The overall objective of the project was better served by expanding the scope of the membrane subproject to develop a hydrogen/methane separation unit, in addition to the methane/carbon dioxide separation unit, than by developing an in-house graphene chemical vapor deposition capability. Therefore, effort was devoted to producing this second membrane unit for the project.

A second hollow-fiber biogas separation module was tested for hydrogen/methane separation. Although not the designed purpose, this membrane is capable of a degree of hydrogen/methane separation, as illustrated in the measured performance in Fig. 5.1-4. This performance could be suitable for the intended methane recycle purpose. However, to achieve higher purity, hollow-fiber membranes tailored specifically to hydrogen/methane separation were acquired.

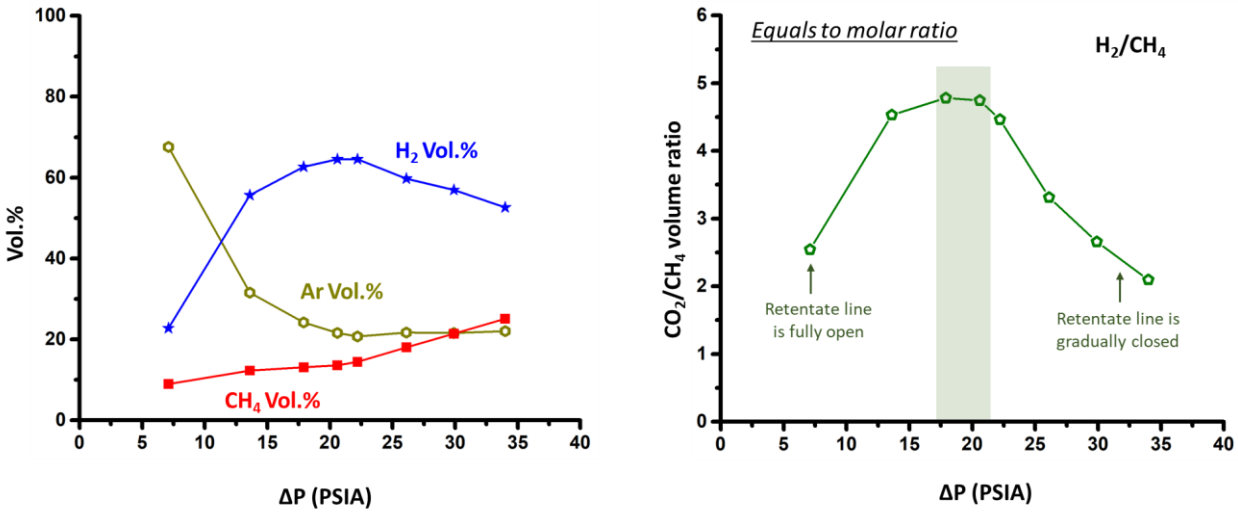

Fig. 5.1-4. Measured performance of hollow-fiber type membrane for hydrogen/methane separation. (left) Gas composition on permeate side vs pressure difference applied across membrane. (right) ratio of carbon dioxide to methane on permeate side vs applied pressure difference.

5.1.3 Membrane integration in demonstration system

With the membrane separation capabilities established, integration of the membrane unit with the non-thermal plasma system was demonstrated in the lab before complete integration at the demonstration site. A schematic of the design is presented in Fig. 5.1-5. Simulated biogas is supplied from gas cylinders upstream and pass through the first membrane unit to create a concentrated methane stream. To maintain a stable flow rate and pressure through the plasma reactor, a buffer tank is installed downstream of the membrane. A small pump circulates gas from the buffer tank through the plasma reactor. Downstream, the produced hydrogen and remaining methane is passed through a second membrane unit to extract the hydrogen while leaving methane behind to circulate back into the buffer tank to recycle through the reactor. The pressure difference in the hydrogen separation membrane unit is created by a pump on the downstream side. Three-way valves are connected at various points in the system to sample the gases and measure composition.

Fig. 5.1-5 shows the membrane units integrated with the plasma reactor. Feed biogas consisting of 60% methane and 40% carbon dioxide is separated by the first membrane unit to produce a >99% pure methane stream supplied to the plasma reactor, as measured by gas chromatography. The supplied flow rate to the plasma reactor is 30 sccm at 15 psi, produced with 40 psi upstream pressure. The plasma reactor converts methane to hydrogen, producing an output stream consisting of 25% hydrogen and the remainder unreacted methane. The hydrogen is extracted by the second membrane unit. The remaining 95% methane is cycled back into the buffer tank to pass through the plasma reactor again, increasing the methane conversion percentage and hydrogen yield. The system with buffer tank installed was tested for several hours on multiple days and showed no signs of performance loss,

membrane degradation, or failure, demonstrating adequate strength and stability for the demonstration system.

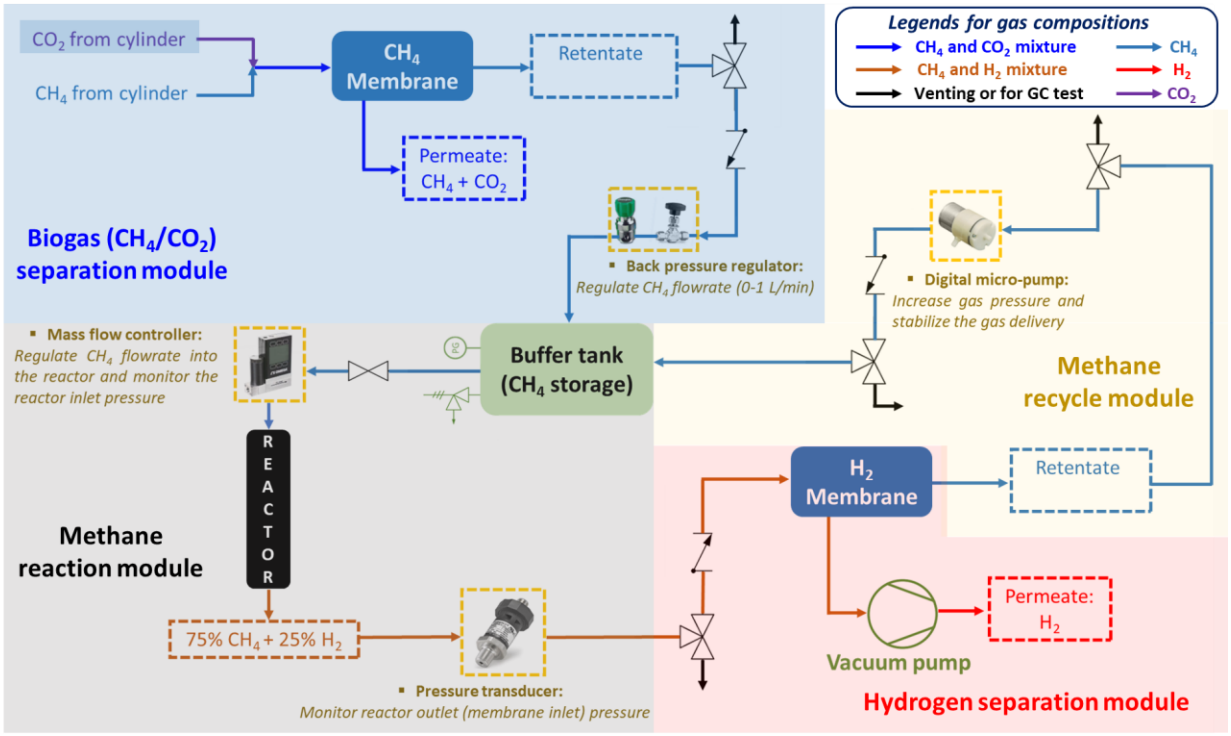

Fig. 5.1-5. Schematic of membrane separation unit integration with non-thermal plasma reactor.

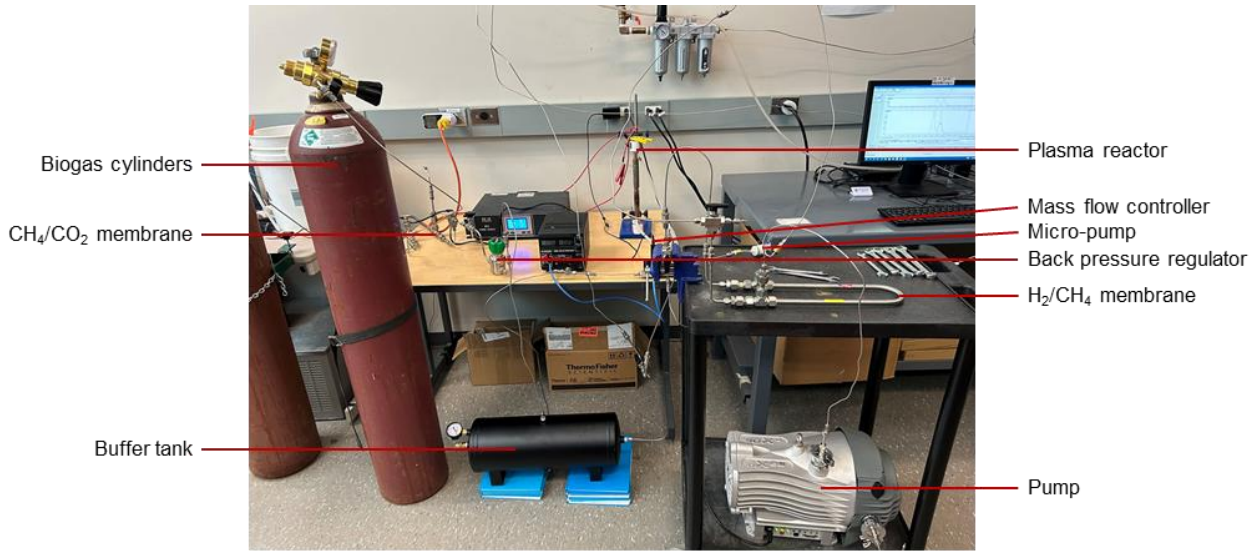

Fig. 5.1-6. Schematic of membrane separation unit integration with non-thermal plasma reactor.

After verifying integration of the membrane unit with the plasma reactor, the two units were moved to the demonstration site and installed in the enclosure pictured in Fig. 5.1-7. The only power requirements for the membrane unit are the two pumps. In the integrated system, this is provided by

the solar panels installed on the roof and sides of the enclosure. The biogas separation membrane module continues to supply high purity methane to the plasma reactor at the demonstration site, but in the integrated system, the separated CO2 is bubbled through the photobioreactor to sequester the carbon.

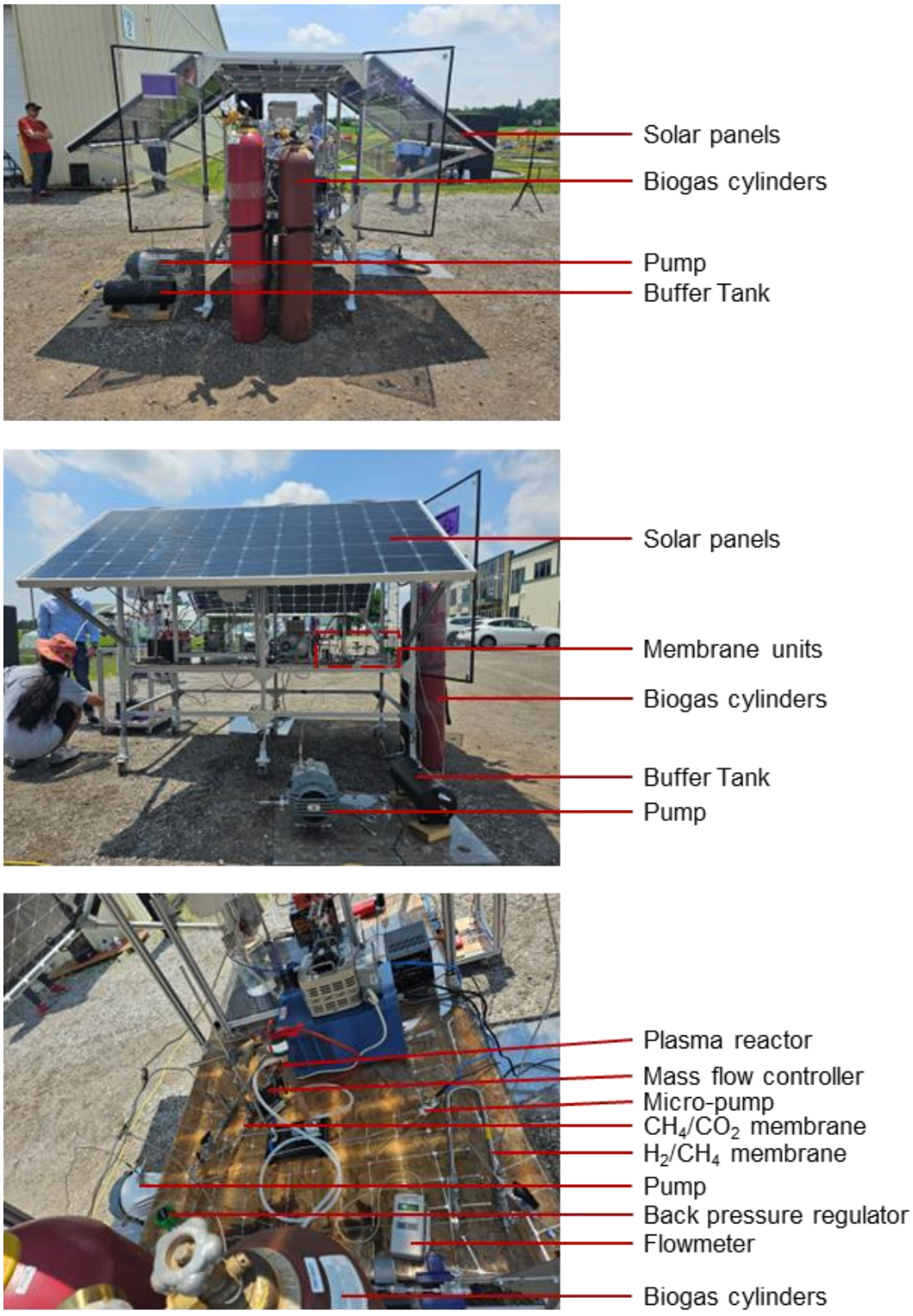

Fig. 5.1-7. Photograph of demonstration unit integration of membrane unit with plasma reactor, photobioreactor, and solar power system.

5.2 Subproject 2: plasma-assisted methene splitting for hydrogen production

A series of fundamental parameters were adjusted to tune the performance of CH_4 splitting, including electrode, voltage, gas composition, and gas flowrate. Furthermore, the length of packing material, the location of packing material, and the type of packing material were studied for improving the CH_4 conversion. The solid byproduct was characterized to explore its potential applications. Finally, the integration of the plasma system with the solar power supply and the graphene membrane separator was demonstrated.

5.2.1 Optimization of technological parameters for improved CH_4 conversion

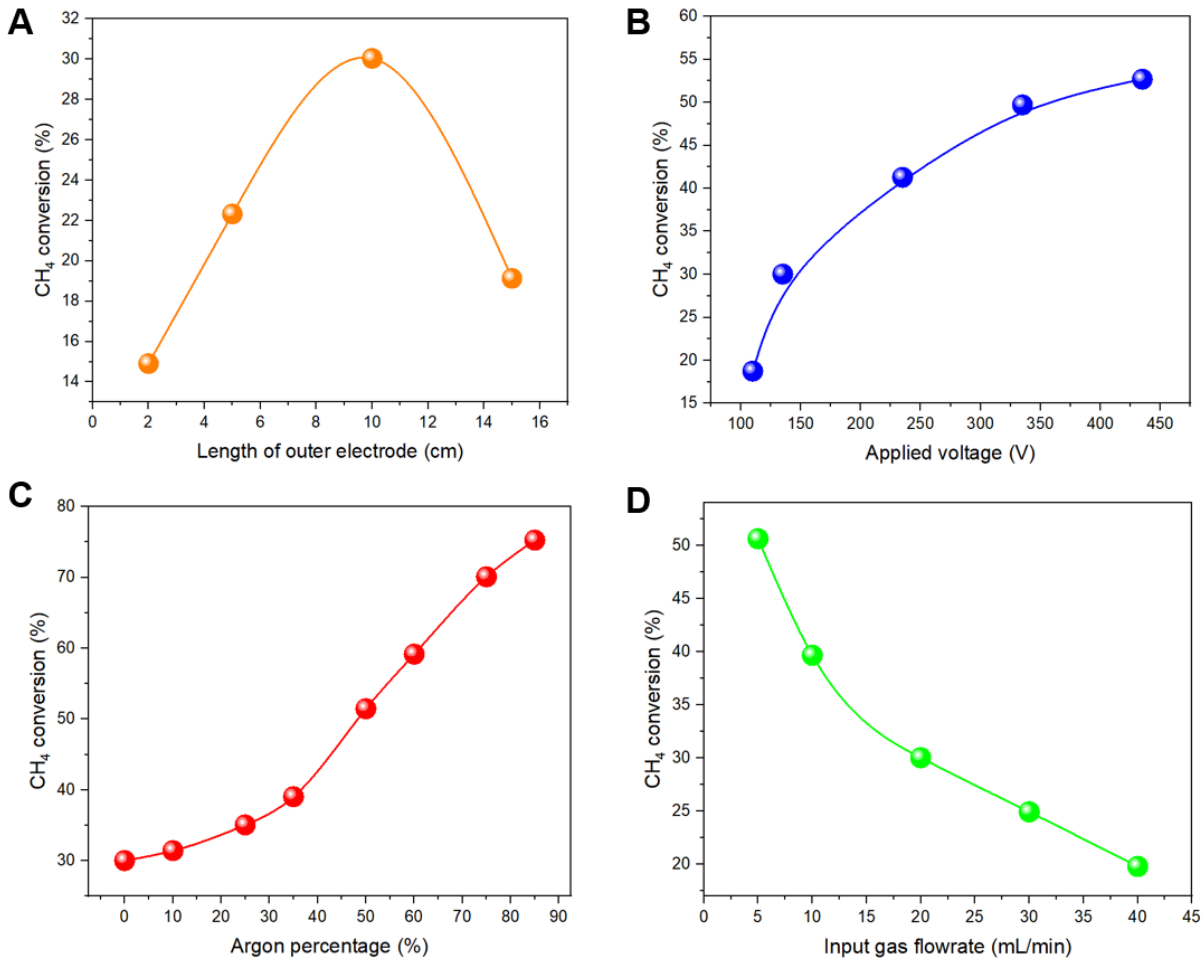

Fig. 5.2-1. Optimization of CH_4 conversion by adjusting the length of outer electrode (A), the applied voltage (B), the Argon percentage in input gas (C), and the flowrate of input gas (D).

The performance of CH_4 splitting is characterized by the conversion (%) of CH_4. A series of technological parameters were explored to improve the CH_4 conversion. These parameters include the length of outer electrode, the voltage applied to the plasma reactor, the Argon concentration mixed with the input CH_4, and the flowrate of input CH_4.

The length of the outer electrode was adjusted to tune the plasma discharge length (Fig. 5.2-1A). It was found that an intermediate discharge length (namely, 10 cm) achieved higher performance than others. This is because the splitting reaction of CH_4 molecules prefers high energy density. In this study, a fixed voltage (135 V) was applied to the plasma reactor, and the obtained current was measured as 0.12 A (unchanged), thus the power energy provided to the plasma reactor was also constant (16.2 W). The excessive long length of outer electrode led to lower performance due to the lower energy density. In addition, the excessive short length of outer electrode limited the total energy applied to the input gas.

Applied voltage was also investigated at a fixed discharge length of 10 cm (Fig. 5.2-1B). One can see that the higher voltage resulted in the higher CH_4 conversion. However, the best energy efficiency (expressed as electricity consumption per unit amount of produced H_2) was found at a relatively low voltage value (135 V) and CH_4 conversion (30 %), with the lowest energy consumption of 585 kWh/kg H_2. At higher applied voltages larger than 135 V, the energy consumption increased significantly because more electrical energy was wasted to produce heat instead of converting CH_4.

Argon was mixed with the input gas of CH_4 to further enhance the excitation and ionization of CH_4 molecules in the plasma region. It can be seen that the conversion of CH_4 was significantly improved after mixing Argon into CH_4 as the input gas to the plasma reactor (Fig. 5.2-1C). However, with the increase of Argon concentration, the production of H_2 decreased significantly. The acceptable Argon concentration was 25%, achieving a relatively high H_2 production rate (11 mmol H_2/h), which is close to that without mixing Argon into the CH_4 (14 mmol H_2/h). Therefore, an Argon percentage of below 25% is recommended for practical applications.

Effects of input gas flowrate was also studied (Fig. 5.2-1D). As shown in the figure, lower flowrate achieved higher CH_4 conversion. This is because the duration of interaction between plasma and CH_4 molecules was extended by using a lower flowrate. However, an intermediate flowrate of 20 mL/min is recommended because lower flowrate produced much less H_2. For example, when the flowrate was decreased from 20 to 5 mL/min, the H_2 production rate was significantly decreased from 14 to 7 mmol/h, even the CH_4 conversion was increased from 30% to 51%.

5.2.2 Evaluate the effects of packing materials on CH_4 conversion

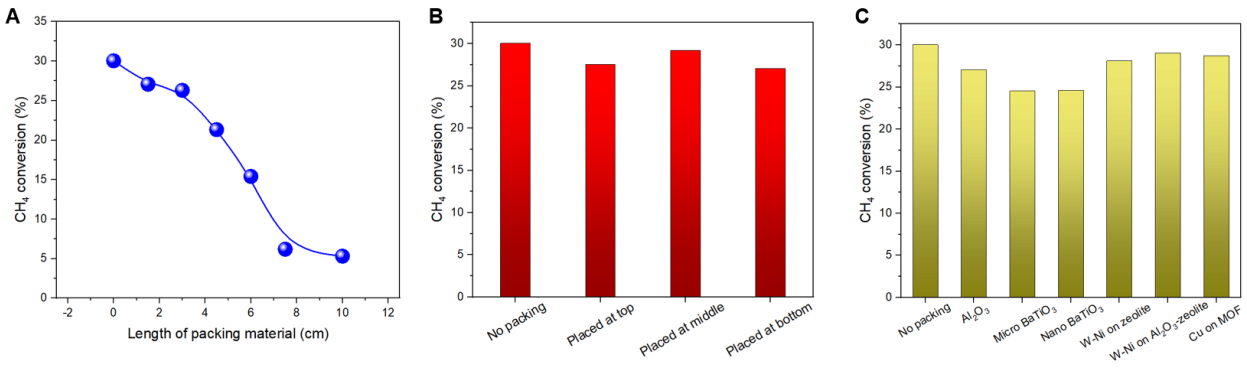

Fig. 5.2-2. Evaluation of packing materials: (A) Effects of packing material length on CH_4 conversion. (B) Effects of packing material location on CH_4 conversion. Note: Al_2O_3 was used as the packing material in these cases. (C) CH_4 conversions obtained by using various packing materials.

Packing materials were filled into the plasma reactor (located at the plasma generation region). This is because the adding of packing material may influence the plasma field to improve the interaction between plasma and the CH_4 molecules. Effects of the length of packing material on CH_4 conversion was investigated and shown in Fig. 5.2-2A. Al_2O_3 powder, a common catalyst support, was used as the packing material. It was filled into the space inside the reactor tube, occupying the interspace between inner electrode and glass tube wall (i.e., plasma discharge region). The existence of packing material could tune the plasma discharge property. The amount of Al_2O_3 powder was adjusted by changing its length (height) in the reactor. As shown in the figure, with the increase of Al_2O_3 powder, the CH_4 conversion decreased significantly. This may be caused by the insulating property of Al_2O_3 which hindered the plasma discharge. Further tuning of Al_2O_3 particles (e.g., particle size, morphology) may improve the performance.

To study the effects of the location of packing material on CH_4 conversion, a fixed amount of Al_2O_3 powder (1.5 cm in length filled in the reactor) was used and placed at different locations (i.e., at the top, the middle, or the bottom of the discharge region). The resulting CH_4 conversions were shown in Fig. 5.2-2B. Compared with the case of no packing, all the cases with the Al_2O_3 packing material showed a slightly lower CH_4 conversion. Notably, when the Al_2O_3 packing material was placed at the middle of the plasma region, the obtained CH_4 conversion was very close to that without Al_2O_3. This is because the plasma-generated energy was fully applied to the Al_2O_3 when it was placed at the middle compared to placing Al_2O_3 at top and bottom. The interaction mechanism between Al_2O_3 and plasma field deserves future studies.

Various packing materials were also employed to study their effects on CH_4 conversion, and the obtained performances were shown in Fig. 5.2-2C. It was found that the catalytic W-Ni metals loaded on Al_2O_3-zeolite support achieved the highest CH_4 conversion of 29%, although this performance is still slightly lower than that without packing material (30%). This indicates the blocking effect of support material on plasma discharge still played the major role. Thus, tuning the particle properties of packing materials is necessary for improved CH_4 conversion. In addition, further development of highly efficient catalytic materials loaded on support materials is needed for boosting the CH_4 conversion.

5.2.3 Characterization of solid carbon material

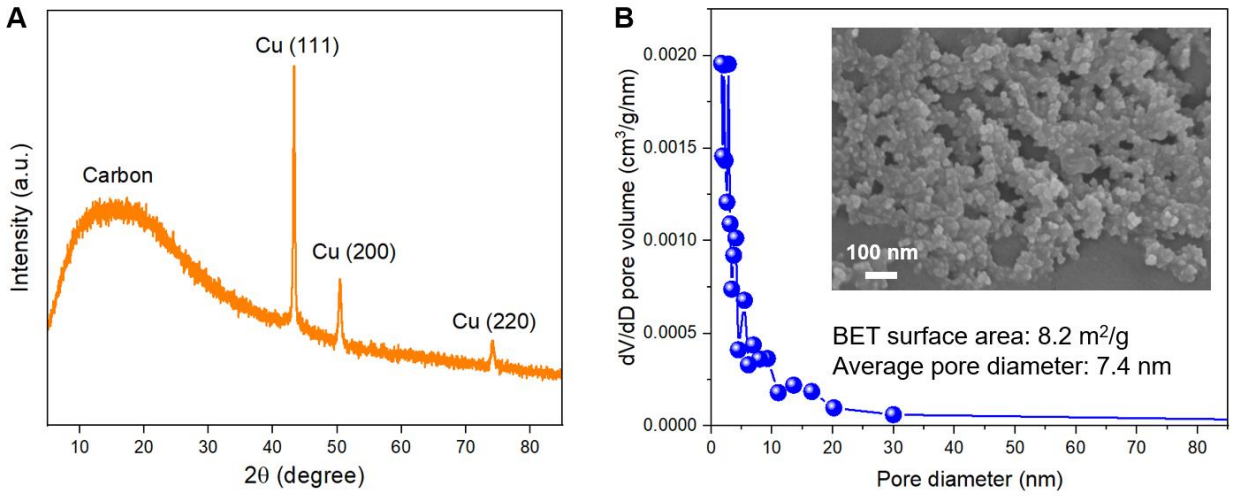

Fig. 5.2-3. (A) XRD pattern of the produced solid carbon powder. (B) BJH pore size distribution, BET surface area, and SEM image of the solid carbon powder.

The as-produced solid carbon powder from CH_4 splitting was deposited on the inner electrode in the plasma reactor during the reaction. After the reaction, the carbon was scraped off and collected for further characterizations. The XRD pattern in Fig. 5.2-3A shows the typical broad peak of carbon, together with well-indexed peaks of copper. The observed copper peaks were from the copper-made inner electrode. The XRD results confirmed the solid product from CH_4 splitting is the carbon.

Pore size distribution measurement (Fig. 5.2-3B) showed an average pore diameter of 7.4 nm. The SEM image in the inset showed uniformly distributed particles. The BET surface area was 8.2 m^2/g, which is lower than typical surface area of carbon black material (at least tens of m^2/g). This could be caused by the agglomeration of the carbon particles during its interaction with the high-energy plasma particles. Further chemical/physical treatments are needed if the carbon will be used for other applications that require high surface area (e.g., electrode of batteries).

5.2.4 System integration and operation demonstration

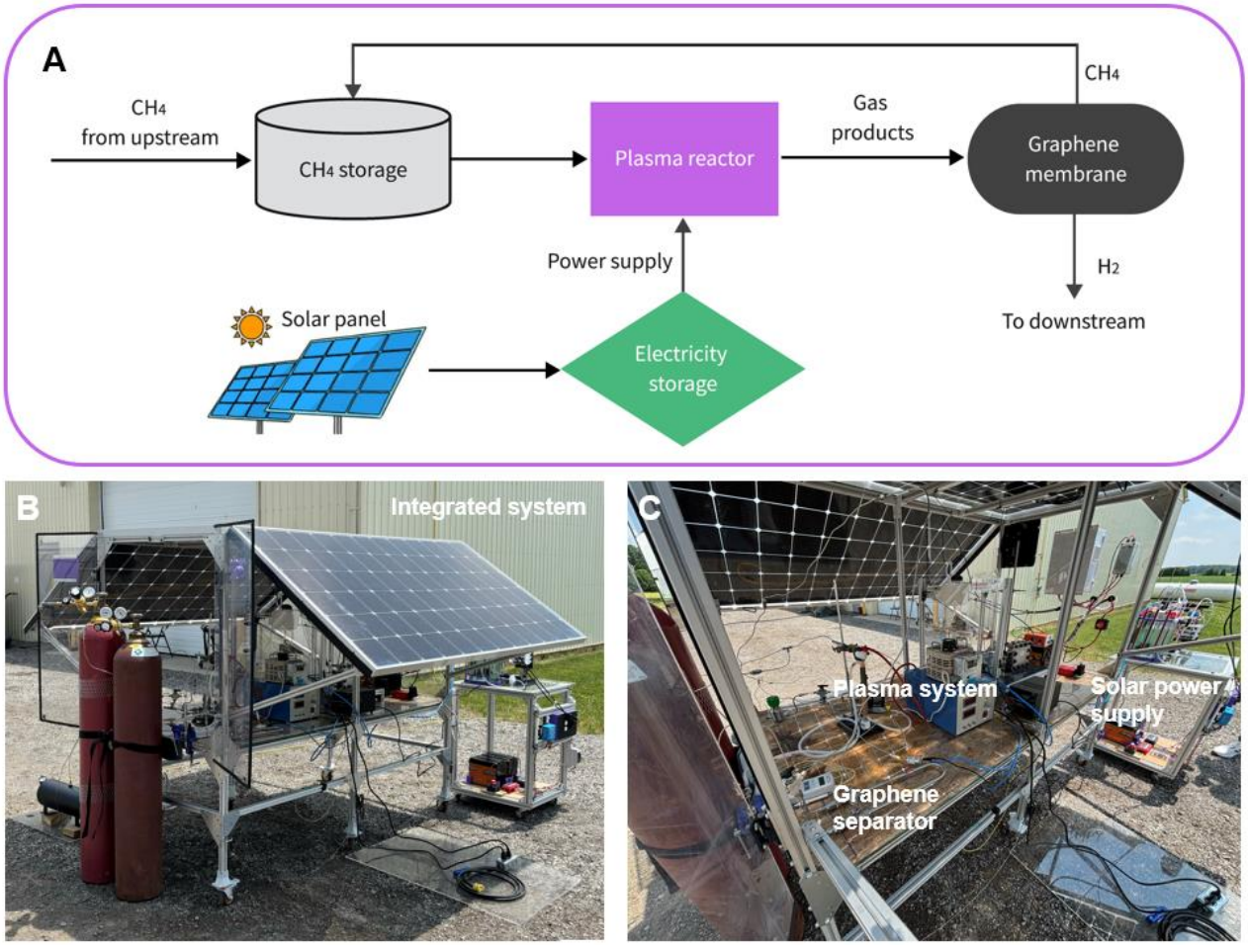

Fig. 5.2-4. (A) Blueprint of the integrated system. (B) Photograph of the as-constructed integrated system. (C) A close view showing the sub-systems consisting of the solar power supply system, the plasma system, and the graphene membrane system.

The compatibility of the plasma reactor-based subsystem with two other subsystems, a solar panel-charged power supply and a graphene membrane separator, was successfully demonstrated. The as-designed blueprint of the whole system is displayed in Fig. 5.2-4A, showing how it is expected to operate. In the system, the portable solar power supply is used as the power source for the plasma generator. Then, the plasma system is driven to operate for H_2 production, and the produced off-gases from the plasma system are collected by the graphene membrane system, where the produced H_2 will be purified for downstream applications, and the unreacted CH_4 will be separated, recycled and reused for the plasma system.

Fig. 5.2-4B shows a photograph of the as-constructed whole system on site. Furthermore, a close view captured at the inner of the system (Fig. 5.2-4C) shows the detailed arrangement of the three subsystems. The integrated system can work steady, and the as-designed blueprint was successfully demonstrated.

5.3 Sub-project 3: PV-AEM electrolyzer

The gas outputs, oxygen (O_2) and hydrogen (H_2), are connected to a condenser and a drier in series to reduce temperature and humidity of the gas produced to measure gas flow were collected and tested for composition in Micro gas chromatography (MicroGC) Varian CP-4900 (California, USA). For gas sampling and testing 1 L gas bags from Environmental Sampling Supply (California, USA) have been used.

Gas flow measurement of H_2 and O_2, first used a gas displacement method with a 3.43 L becher and timing the time to fill it with gas. In subsequent tests, gas flowmeters with completely opened valve have been calibrated to have a constant gas flow reading. For this purpose, several measurements have been conducted in parallel to find the multiplication factor for the specific gas flowmeter. For H_2 the value calculated is 3.25 while for O_2 is 1.25 and another factor calculated from gas temperature has been calculated from Charles's Law (Equation 1).

$$\frac{V_1}{T_1} = \frac{V_2}{T_2} \tag{1}$$

$$Gas\ Flow\ Adjusted = \frac{F * c}{k} \tag{2}$$

F is the gas flow read by the flowmeter, c is the calibration factor found comparing the measurements equal to 3.25 and k is the temperature factor correction given by the temperature registered and STP value.

The tests made were several with the purpose of characterizing the AEM electrolyzer stack, its output and efficiency. From the data collected over the AEM has been possible to extrapolate the stack efficiency, η, determined by Equation 3:

$$\eta\ (\%) = \frac{\mathrm{HHV\ H_2}}{E} * 100 \tag{3}$$

Where the high heating value (HHV) of 1 kg H_2 which is 39.4 kWhr, E is energy consumption and is calculated over Equation 4

$$E = P * t = (V * I) * \left(\frac{Vol}{F} \times k\right) \tag{4}$$

Energy is calculated as power, given by voltage (V) and current (I) used, by time calculated to produce 1 kg of H_2 (Vol, volume occupied by 1 kg of H_2) using the gas flow of the AEM (F).

In a test in which the electrolyzer has not been heated from external heat exchangers has been possible to calculate the thermal efficiency (η_T) of the stack using Equation 5:

$$\eta_T\ (\%) = \frac{E-H}{E} * 100 \qquad (5)$$

The electrical results are shown in Figure 5.3.1, strictly relating voltage and current values to the temperature of the electrolyte. As the temperature increases the voltage drops from 48.5 V to 47.4 V while the current draw rises to 100 Amps which represent the upper bound of this specific AEM cell. Figure 5.3.2 shows the flowmeters measurements for H_2 and O_2 in parallel with the power consumption and the temperature all as a function of time.

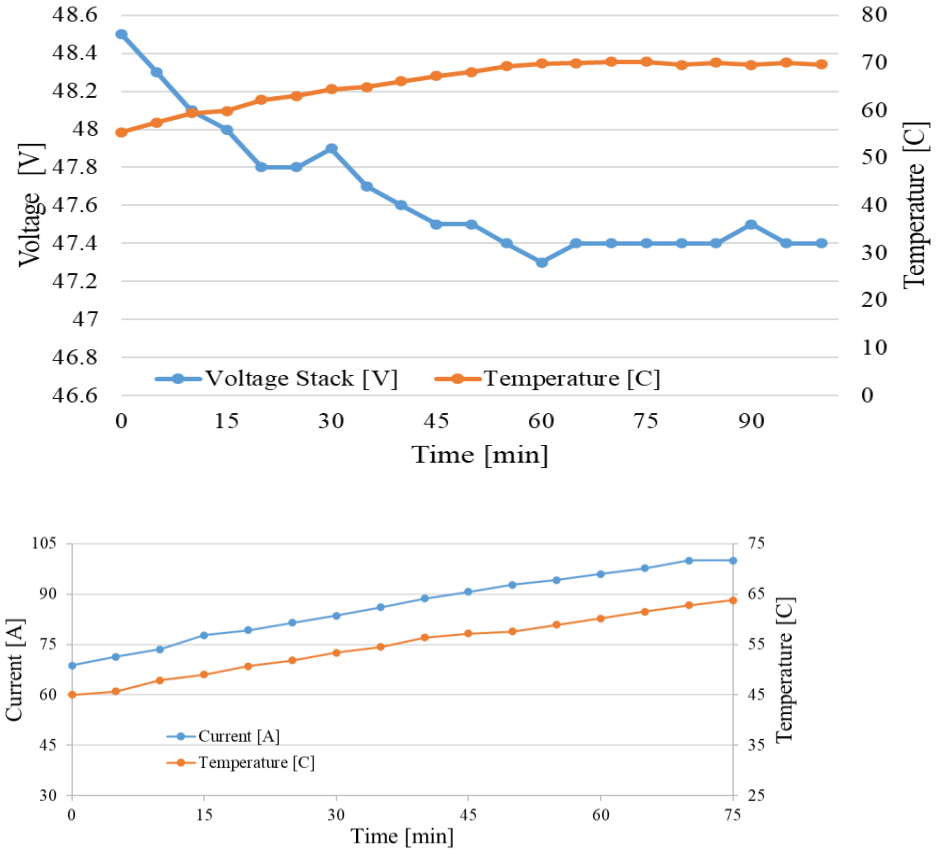

Figure 5.3.1 : voltage, current and temperature in the electrolyzer as a function of time

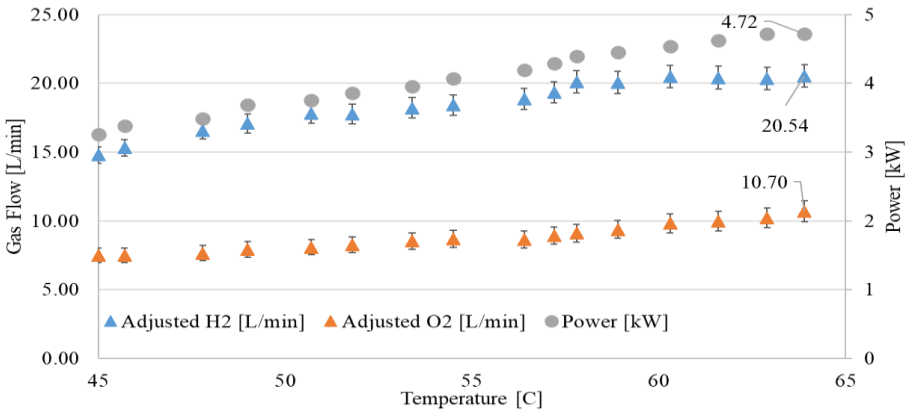

Figure 5.3.2. Gas flow measurements and power as a function of temperature in the AEM electrolyzer

Figure 5.3.3 shows the energy efficiency correlated to the power consumption (Figure 5.3.3a) as a function of temperature. There is a peak of 86% and an overall average of 80%. Thermal efficiency (Figure 5.3.3b) is increasing with the temperature rise and it is well and consistently above 90% with a peak of 98.4 % when the temperature reaches 65 °C.

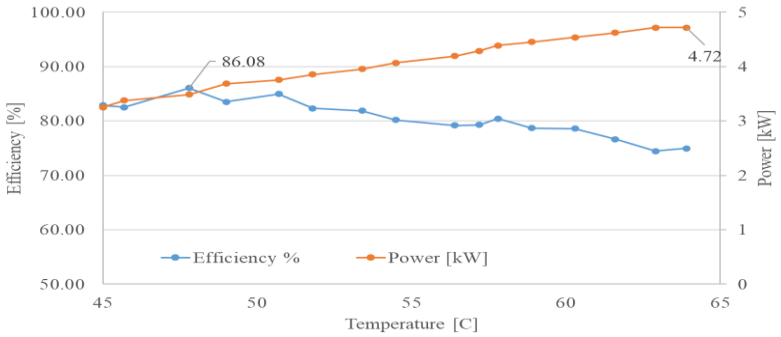

(a)

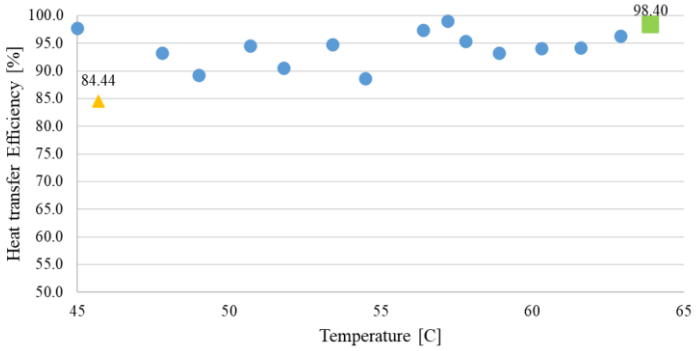

(b)

Figure 5.3.3 a) energy efficiency and b) heat transfer efficiency.

Table 1 show the average hydrogen production from the AEM electrolyzer..

Table 1. Hydrogen output and oxygen output composition.

	H_2 [%]	O_2 [%]
Hydrogen output	99.119	0.58
	99.215	0.61
	99.167	0.44
Average	**99.167**	0.544
Oxygen output	3.437	96.72
	3.418	97.20
	3.440	97.64
Average	3.428	**96.958**

Integration into the Grid System Overview

The electrolyzer system, powered by solar panels, successfully produced 1000 liters of hydrogen per hour at CN. To utilize this hydrogen for electricity generation, we can couple the system with a Proton Exchange Membrane (PEM) fuel cell.

Fuel Cell Sizing

Based on the hydrogen production rate of 1000 liters per hour (approximately 90 grams of hydrogen), and assuming a PEM fuel cell efficiency of 70%, a fuel cell with a capacity of approximately 5 kW would be appropriate.

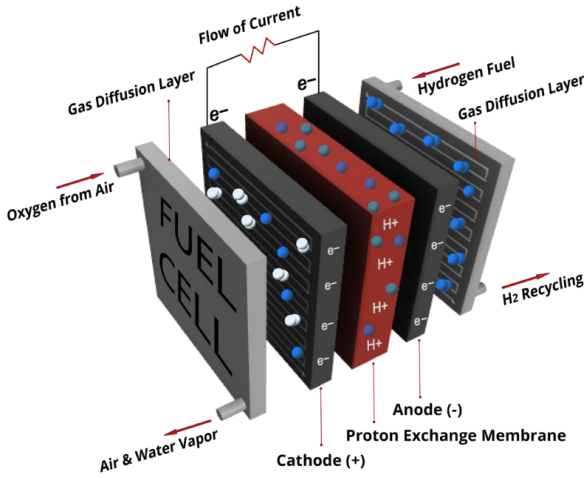

Figure 5.3.4 PEM fuel cell

Electricity Generation Potential

With a fuel cell efficiency of 70%, the electricity generation potential is as follows:

- **Hydrogen Energy Content:** 90 grams of hydrogen can produce approximately 3 kWh of energy in a fuel cell at 100% efficiency.
- **Adjusted for 70% Efficiency:** At 70% efficiency, the fuel cell would generate approximately 2.1 kWh of electricity per hour.

Over a 24-hour period, this would equate to 50.4 kWh of electricity under optimal conditions.

Yearly Contribution to the Grid

Assuming continuous operation, the yearly contribution of electricity to the grid would be 50.4 kWh/day × 365 days = 18,396 kWh per year. This amount of electricity can power several homes for a significant portion of the year, depending on local consumption patterns, and represents a meaningful addition to the grid from a renewable source.

Electricity Consumption of the AEM Electrolyzer

It should be noted that one of the strengths of the DC process is that it is far more efficient to go from PV to AEM to hydrogen directly in DC rather than convert first to AC or to use AC directly (e.g., the small-scale system is the way larger grid-tied systems should operate). If the AEM electrolyzer were powered by AC electricity instead of solar panels, however, we would need to consider its electricity consumption:

- **Hydrogen Production Rate:** 1000 liters per hour (approximately 90 grams or 0.09 kilograms of hydrogen)
- **Electricity Consumption:** 49.25 kWh per kilogram of hydrogen produced

For 1000 liters (0.09 kilograms) of hydrogen:

- **Hourly Electricity Consumption:** 0.09 kg × 49.25 kWh/kg = 4.43 kWh of electricity

Over a 24-hour period, this would equate to:

- **Daily Electricity Consumption:** 4.43 kWh/hour × 24 hours = 106.32 kWh per day
- **Yearly Electricity Consumption:** 106.32 kWh/day × 365 days = 38,806.8 kWh per year

Net Impact on the Grid

Given that the electrolyzer consumes 4.32 kWh to produce the hydrogen that can generate 2.1 kWh of electricity, there is a net electricity consumption of:

- **Net Electricity Usage:** 4.43 kWh (consumed) - 2.1 kWh (generated) = 2.33 kWh of electricity used per hour.

On an annual basis:

- **Yearly Net Electricity Usage:** 2.33 kWh/hour × 24 hours/day × 365 days = 20,410.8 kWh per year.

5.4 Sub project 4- Results and Analysis

Figure 5.4.1 below describes the cultivation of the *Chlorella* microalgae in the 7L photo-bioreactor. The objectives were to investigate the removal of nutrients from a simulated waste-water stream

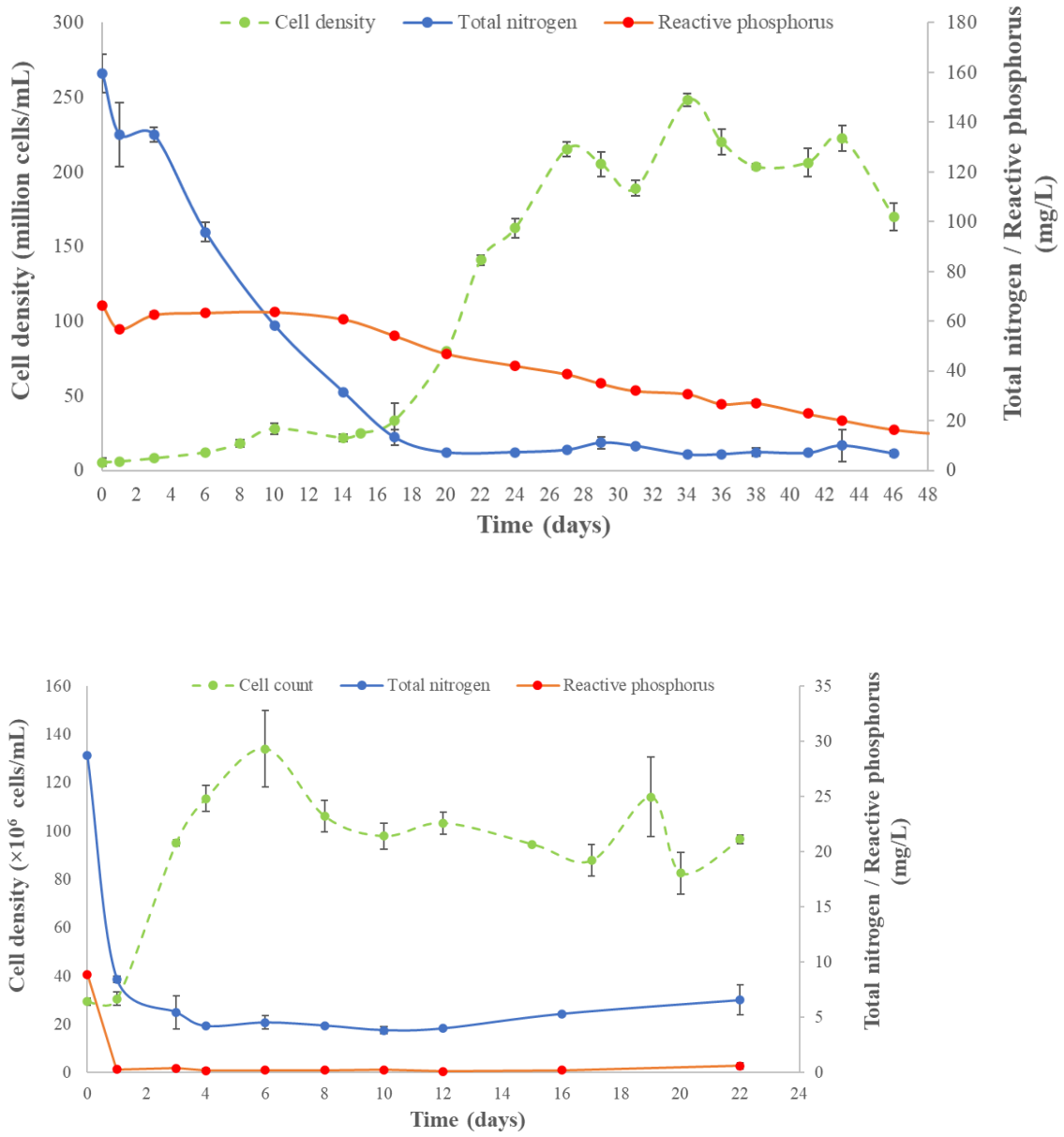

Figure 5.4.1: **Chlorella** growth kinetics in a 7 L bubble column. The top figure is using a mixed feed of fertilizer and frass and the lower figure is for acclimated Chlorella microalgae growth on frass waste.

As shown above the chlorella were able to complete remove nitrogen and phsophrus from the waste water stream in the presence of carbon dioxide as a carbon source. Air was used as a source of the

carbon dioxide. Eco-plastic prepared from the microalgae was tested for stiffness using various combinations of ingredients.

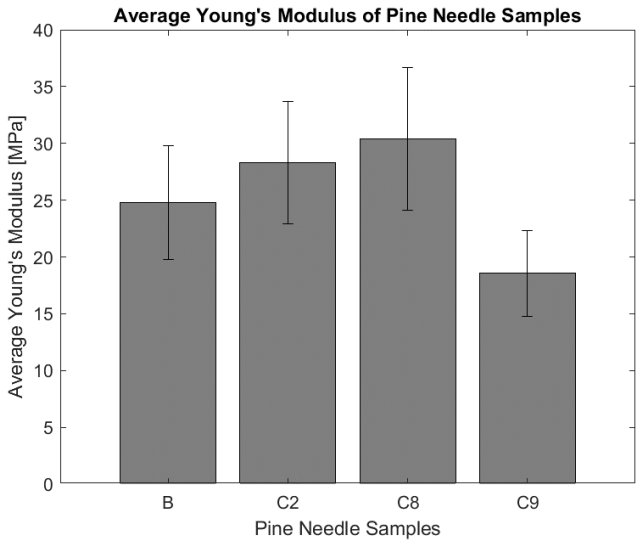

Figure 5.4.2 : Young's modulus as a function of bioplastic composition.

6 Discussion

Green Hydrogen production: This analysis shows that while the system can generate electricity, it consumes more electricity than it produces when the AEM electrolyzer is powered by AC power. **Thus this system works better as a way to obtain green solar energy on demand.** Additionally, this system can contribute to grid balancing by generating hydrogen during off-peak hours and converting it back to electricity during periods of peak demand or high grid load.

In this study we demonstrated the extreme of operating the PV off-grid and converting the solar electricity to hydrogen after first being converted to 3-phase AC, which could be stored to produce electricity when needed. We envision the next generation would be grid attached but that the power for the AEM would be direct DC from the PV, and only used through the fuel cell to inject electricity when financially viable, otherwise to store the energy as hydrogen to produce electricity when it becomes more favorable.

Grid Injection

To inject the generated electricity into the grid, the following steps can be implemented:

- **Inverter Integration:** The DC output from the fuel cell will need to be converted to AC using a grid-tied inverter. The inverter should be sized according to the fuel cell's output, in this case, approximately 3 kW considering the efficiency.
- **Grid Connection:** The inverter will be connected to the local electrical grid. The system must be synchronized with the grid's voltage and frequency, ensuring that the power is injected seamlessly.

Regulatory Compliance: The injection of electricity into the grid requires adherence to IESO regulations, including grid codes, safety standards, and metering requirements. Coordination with the local utility is essential to ensure proper integration

By coupling the electrolyzer with a fuel cell, the system can convert excess energy into storable hydrogen and subsequently generate electricity on-demand. This enhances grid stability and provides an energy source that can be dispatched as needed. The system can also support peak shaving, grid balancing, and provide backup power.

This analysis demonstrates the potential for integrating hydrogen production and fuel cell technology with the existing grid infrastructure, offering a pathway to more sustainable and resilient energy systems.

Blue Hydrogen: The three components of blue hydrogen production from methane were clearly demonstrated at bench scale. First a simulated mixture of biogas (methane and carbon dioxide) was completed separated using commercial and graphene membranes, When the CO_2 is used as a carbon source my microalgae, the carbon is incorporated into biomass. Theoretically every Kg of microalgae can sequester 1.8 Kg of carbon dioxide. A 20000 L bioreactor contains 20 – 40 Kg of biomass and therefore can sequester 36 to 72 Kg of carbon dioxde if all the biomass is converted to bioplastic, The plasma system produces carbon black and hydrogen and over a net negative carbon footprint process is shown. Using a PV system to operate both the photobioreactor and plasma reactor can help to alleviate the large energy demand f these systems.

7 Economic/Technical Impact, and Risk Assessments

Two of the sub projects were operated at bench scale (membrane separation and plasma reactor) and scale up was not considered due to the one year mandate and with the main goal of demonstrating the feasibility of the proposed concept. Thus a large scale economic analysis of the integrated process was not carried out as it will require a knowledge of efficiencies of hydrogen production at scale up of the plasma system.

Risk assessment: The lack of sufficient information on scaling up the plasma reactor can lead to uncertainties in terms of energy demand. Thus the plasma technology is currently requiring more research and development. The other three components: PV-AEM electrolyzer, membrane separation of biogas and large scale microalgal cultivation are technology ready projects which can be implemented at large scale at low economic risk. The benefits of GHF reduction (methane and carbon dioxide) , reduction of water footprint by water recycle and potential economic value by producing eco-plastic or other high value nutraceuticals makes the combine approach low risk and economically attractive. Future work is necessary to appropriately determine economic impact but the reduction in the environmental impact is demonstrated by the data that we collected.

Life Cycle Assessment

Life cycle assessment (LCA) is a scientific methodology used to determine the possible environmental consequences of a product, process, or system across its entire lifespan, starting from the extraction of raw materials and ending with its disposal. The hydrogen LCA model and carbon intensity measurement is based on a comprehensive life cycle methodology that considers all stages of hydrogen production, encompassing the acquisition/extraction of raw materials, production and transportation of feedstock, and the actual hydrogen production process. The main objective is to perform a carbon footprint analysis, specifically to determine the degree to which hydrogen production contributes to global warming (GWP) in terms of CO2e. This will be achieved by measuring the greenhouse gas (GHG) emissions at each stage of the process, in accordance with the guidelines outlined in ISO 14040:2006, 14044:2006, and 14067:2018. The production will utilize a consistent functional unit of 1 kilogram of hydrogen. The carbon footprint is measured in kilograms of carbon dioxide equivalents (kg CO2e) for each kilogram of hydrogen produced. Additionally, the energy demand will be evaluated and quantified as kilowatt-hours per kilogram of hydrogen produced. The system boundary approach that encompasses all the components of the hydrogen value chain is referred to as the "well-to-gate" approach. This approach takes into account all the available alternatives at each point of the life cycle, starting from the procurement and transportation of raw materials to the production of hydrogen. The LCA research was conducted using the open-source program openLCA, which was developed by Green Delta. The carbon footprint is calculated using the IPCC GWP 100a technique, whereas the aggregated energy demand is determined using the Cumulative Energy Demand method

Producing 1 kilogram of gray hydrogen requires 159 kWh of electricity, with approximately 94% of the total greenhouse gas (GHG) emissions attributed to this process. The manufacturing of gray hydrogen relies on electricity generated from fossil fuels. The carbon emissions associated with gray hydrogen production amount to 41.87 kg CO2 eq. per kilogram of H2. Conversely, blue hydrogen, green hydrogen, and pale blue hydrogen require 80%, 99%, and 88% less energy, respectively, compared to gray hydrogen. Figure 7.1 displays the total energy requirement for various ways of hydrogen production.

The blue hydrogen utilizes around 1,456 kWh of on-site electricity generated by a solar PV system. The emission associated with the electricity is approximately 9 kilograms of carbon dioxide equivalent per kilogram of hydrogen. Nevertheless, since blue hydrogen relies on biogas as its main source and incorporates carbon capture storage, about 5.7E08 kilogram CO2 eq./ kg H2 may be eliminated from the environment. Furthermore, a total negative carbon footprint of -7.06E08 kg CO2 eq./ kg H2 has been recorded. During the production of green hydrogen, about 70.21% of emissions are attributed to the usage of carbon-intensive electricity and transportation for the manufacture of green electricity and KOH solution. Nevertheless, the total emission is 99.27% lower than that of gray hydrogen. The pale blue hydrogen, which is a combination of blue hydrogen and green hydrogen, possesses a negative carbon footprint. Figure 7.2 displays the carbon footprint associated with various forms of hydrogen.

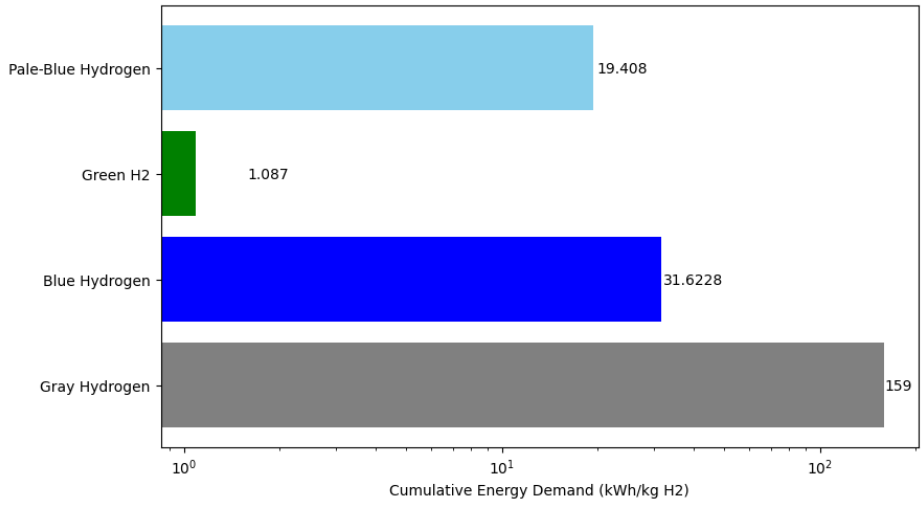

Figure 7.1. Cumulative energy demand for different types of hydrogen. Note the pale blue hydrogen value is dependent on the mixing ratio between blue and green hydrogen. Note this is a log scale graph.

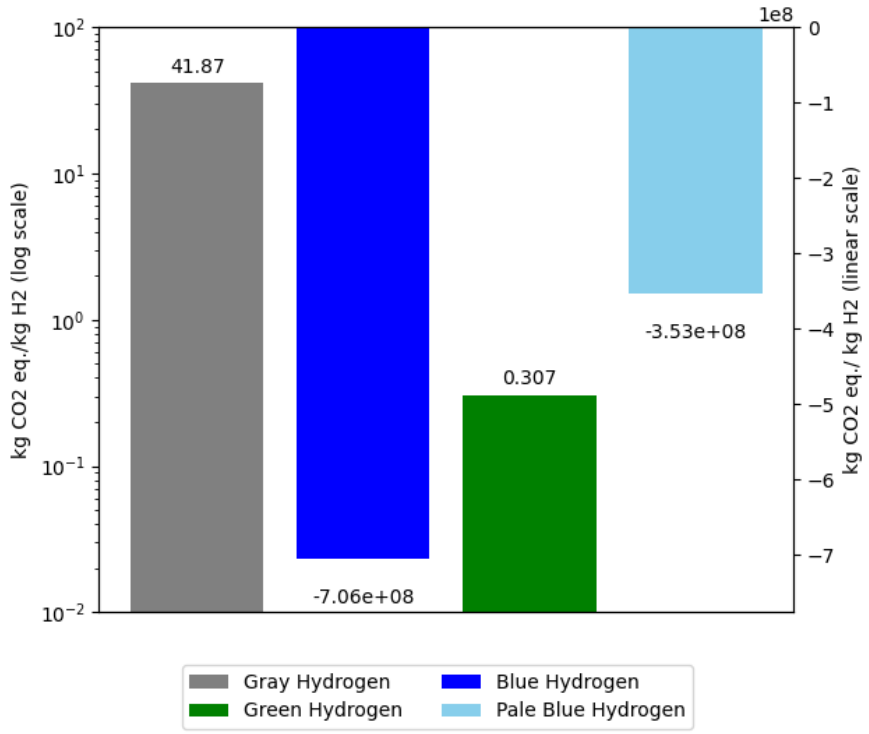

Figure 7.2. The mass of carbon dioxide per kg of hydrogen for the different types of hydrogen.

The carbon footprint of pale-blue hydrogen is determined by the proportion of blue hydrogen and green hydrogen in 1 kg of pale-blue hydrogen. Green hydrogen has a carbon footprint that is positive, while blue hydrogen has a carbon footprint that is negative. The greater the amount of blue hydrogen, the

more carbon-negative the pale blue hydrogen will become. Figure 7.3 displays the carbon footprint associated with various proportions of blue and green hydrogen in pale-blue hydrogen.

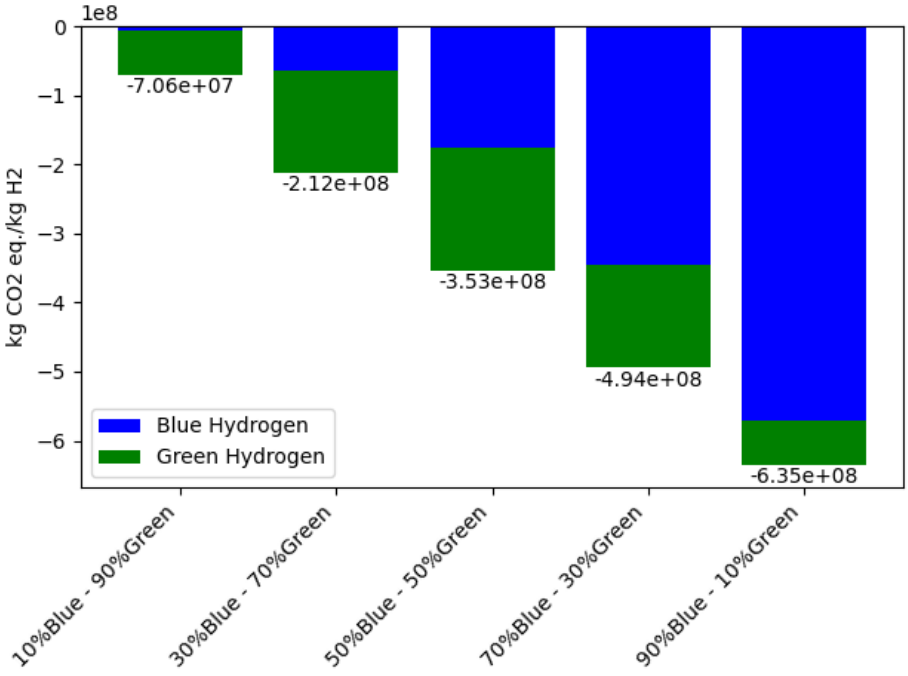

Figure 7.3 Carbon footprint associated with various proportions of blue and green hydrogen in pale-blue hydrogen.

Total Energy Consumption (kWh/kg H_2) for Complete System: Comprehensive Electrical Requirements for Producing 1 kg of Pale Blue Hydrogen

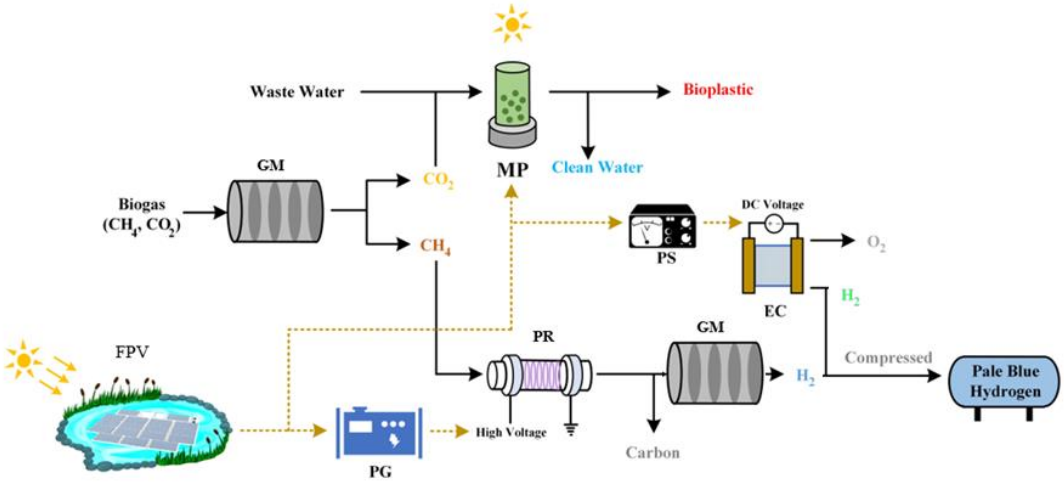

Figure 7.4. Flow diagram of pale-blue hydrogen production

In this experimental setup (Figure 7.4), the entire hydrogen production process is powered by a solar photovoltaic system, engineered to enable carbon-negative hydrogen generation. The system operates with two distinct hydrogen production streams, each incorporating multiple power-dependent components. The total power requirements for each stream and its subsystems are outlined below:

1. AEM-Based Green Hydrogen Production

- Losses in the DC-DC converter
- DC pump power consumption for electrolyte circulation
- Electrolyzer power consumption

2. Plasma System Power Consumption

- Power for methane separation from biogas
- Power required by the plasma reactor
- Internal losses in the plasma generator

The total energy demand for the production of 1 kg of hydrogen across these two streams (in this small-scale setup) is summarized below, accounting for all stages of power consumption.

	AEM electrolyzer produced H_2	**Plasma produced H_2**
Energy Consumption/1Kg H2	74.17 kWh	585 kWh
Water required/ 1kg H2	12 kg	-
KOH required/ 1kg H2	1.2 kg	-
Overall Efficiency	45%	2.29%

The following section presents a detailed calculation of the total energy required for hydrogen production in each stream.

1. H_2 produced by AEM Electrolyzer:

The electrical characteristics of AEM while the electrolyzer was working at 20^0-30°C, is shown in Figure 5(a). In 7.5(b) the results obtained in terms of gas production measured through the flowmeter is displayed.

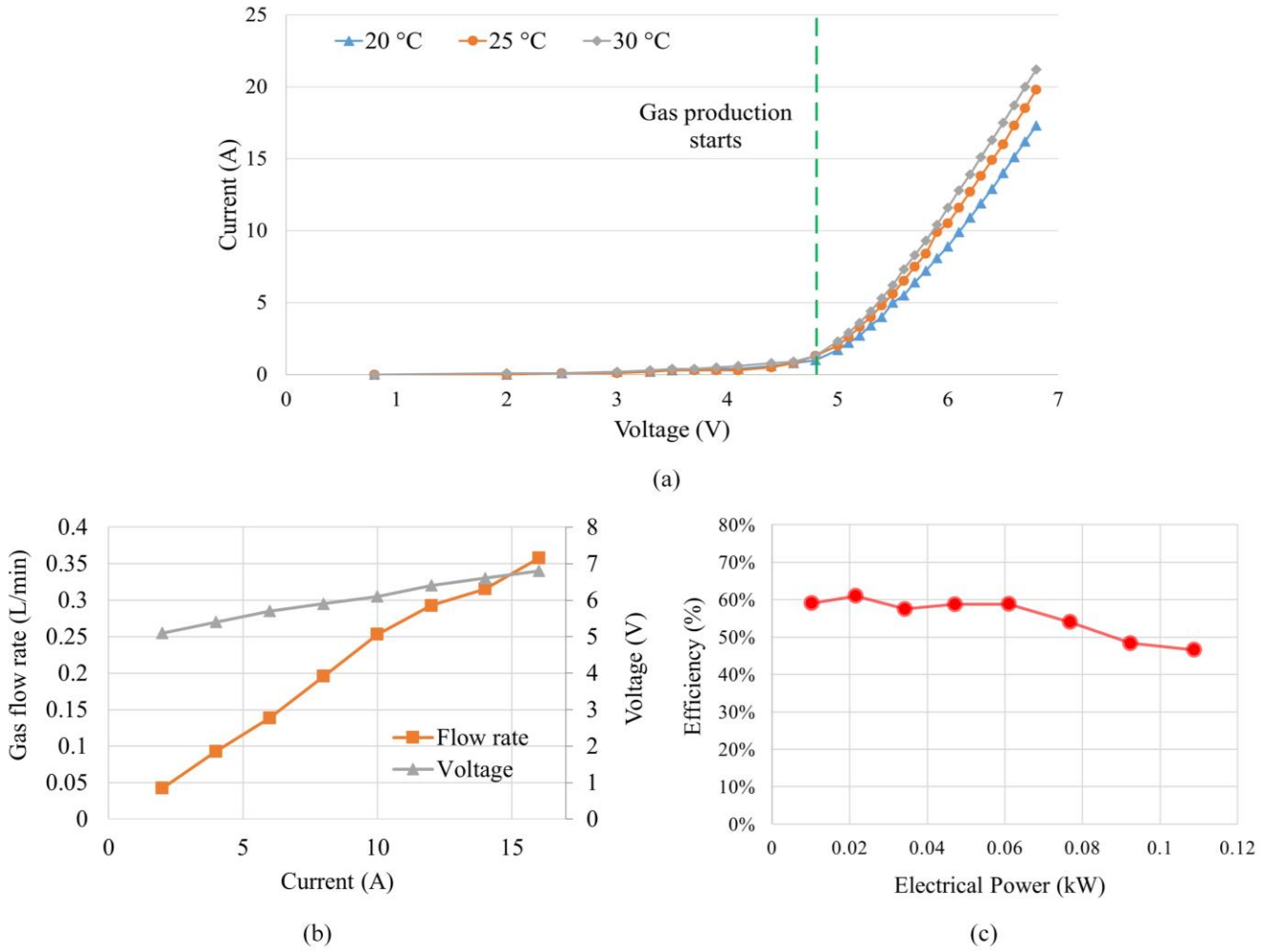

Figure 7.5. (a) Current vs voltage characteristics curve of AEM electrolyzer; (b) Gas flow measurements and (c) Efficiency vs power consumption of AEM.

Many studies on renewable hydrogen production systems overlook the significant variation in electrolyzer efficiency with changes in input power. Figure 7.5(c) demonstrates that AEM electrolyzer efficiency decreases as the load increases. The maximum efficiency of 60% is achieved at a current of 10A (60W). For this study 10A is considered as optimum operating current and the AEM is operated at this current for 60 minutes for both the grid connected and off-grid PV setup at the same 10A current. The two setups are directly compared based on measuring the flow rate in each in three minute interval. Throughout the period of experiment for the setup the flow rate of hydrogen is found to be around 0.25 L/min.

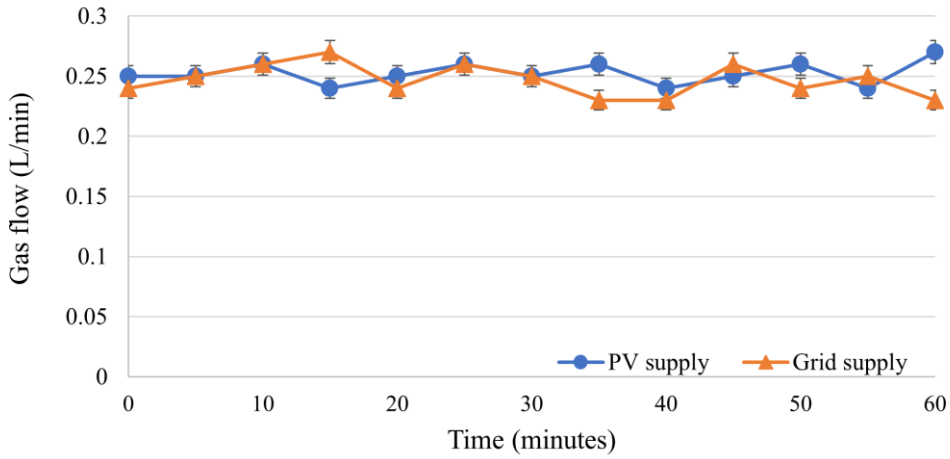

Figure 7.*6*. Flow rate vs time (grid vs off grid).

This setup, in those conditions consistently achieves an average flow rate of 0.25 L/min (15 L/hr) (Figure 7.6) while the total power consumption by the electrolyzer process including pump, sensors, DC-DC converter internal losses total 0.1 kWhr of energy consumption which is equivalent to 74.17 kWhr/kg of H_2, utilizing 12 kg of water and 1.2 kg of potassium hydroxide (KOH) as a catalyst.

2. H_2 produced from plasma:

The voltage value can be set by the panel on the plasma generator. By applying this voltage on the two electrodes of the plasma reactor, the current value can be measured by the plasma generator itself and shown on its screen. Thus, the actual power applied on the plasma reactor can be calculated by the product of the applied voltage and the detected current.

- Comparative analysis between a grid-connected plasma generator and the portable power supply connected mode.

The performance of CH_4 splitting reaction ($CH_4 \rightarrow C + 2H_2$) in plasma reactors can be evaluated by the following parameters:

(1) CH_4 conversion (%) =

$$\frac{\text{moles of } CH_4 \text{ input} - \text{moles of } CH_4 \text{ output}}{\text{moles of } CH_4 \text{ input}}$$

(2) H_2 production rate (mL min^{-1})=

$$\frac{\text{moles of } H_2 \text{ produced (mol)}}{\text{gas collection time (min)} \times \frac{1}{24500}\ (\text{mol mL}^{-1})}$$

Note: the volume of 1 mol gas at 1 atm and room temperature (25 °C) is 24,500 mL.
The moles of input/output gases can be measured using gas chromatograph (Shimadzu Corp., GC-2014). Then, the CH_4 conversion and H_2 production rate can be used for evaluating and comparing the performances of the grid-connected plasma generator and the portable power supply-connected plasma generator. In addition to gas products analysis, solid products will be analyzed by X-ray diffraction (XRD, Rigaku Corp., SmartLab) for phase identification, scanning electron microscope (SEM, Hitachi Ltd., SU8230) for morphological analysis, X-ray photoelectron spectroscopy (XPS, Kratos Analytical Ltd., AXIS Supra) and Fourier transform infrared spectrum (FT-IR, Thermo Electron Corp., Nicolet 6700) for chemical composition analysis, as well as N_2 adsorption-desorption isotherm (Micromeritics Instrument Corp., ASAP2020 Plus) for quantification of pore size distribution, specific surface area, and porosity.

- A case study of CH_4 splitting performance measured at various power values:

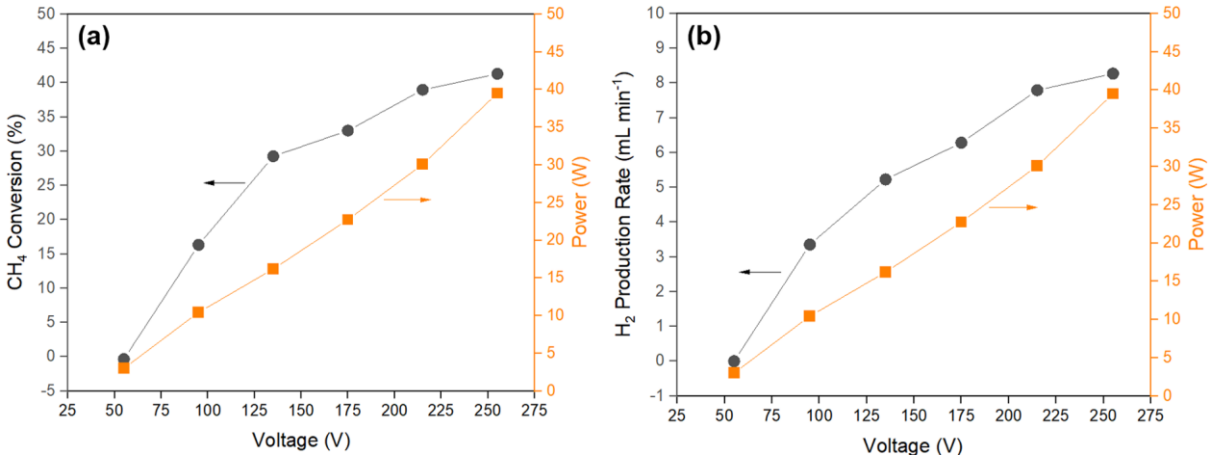

Fig.7.7. (a) CH_4 conversion and (b) H_2 production rate for CH_4 splitting measured in the DBD plasma reactor at various power values.

The performance of CH_4 splitting has been measured at various power values using the grid supply. Firstly, a voltage value was set for the plasma generator. By applying this voltage on the DBD plasma reactor, a current value can be obtained. Then, the actual power applied on the plasma reactor can be calculated by the product of the applied voltage and the detected current. Based on this method, a series of voltage values (see X-axis of **Fig.7**.7) were applied on the plasma reactor, and the corresponding power values were calculated and shown on the right Y-axis. Under these conditions, CH_4 conversion and H_2 production rate were measured and shown on the left Y-axis. One can see that both CH_4 conversion and H_2 production rate increased with the increased power.

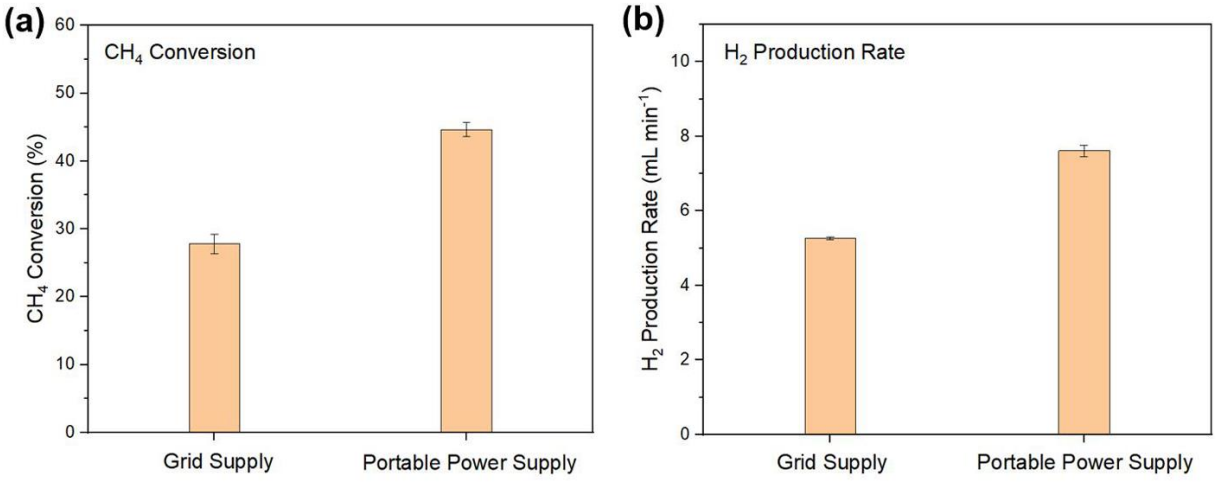

(c)

	Grid Supply	Portable Power Supply
Set Voltage (V)	135	135
Actual Voltage (V)	135	120-140 (fluctuant)
Actual Current (A)	0.12	0.12-0.17 (fluctuant)
Actual Power (W)	16.20	18.85 (average)

Fig. 7.8. (a) CH_4 conversion and (b) H_2 production rate obtained by grid supply and portable power supply. (c) Electrical parameters recorded during the tests.

The performance of CH_4 splitting was also measured using the portable power supply, and a comparison of the performances generated by the portable power supply and the grid supply is summarized in Fig. 7.8 (a-b). The initial voltage was set as 135 V for both cases. As seen in Fig. 6 (c), the resultant voltage produced by the portable power supply ranged from 120 V to 140 V, while the generated current ranged from 0.12 A to 0.17 A, resulting in an average power output of 18.85 W. Additionally, the CH_4 conversion rate reached 44.67%, with an H_2 production rate of 7.61 mL min^{-1}, both higher than the values obtained from the grid supply (27.83% and 5.26 mL min^{-1}, respectively).

H_2 production:

For off-grid hydrogen production using a plasma reactor, the production rate is 7.61 mL/min with a power consumption of 18.85 W, equating to approximately 460 kWh per kilogram of hydrogen. However, this calculation excludes internal losses within the plasma generator, which are addressed in the subsequent section on total energy requirements.

Total energy consumption including Methane separation from biogas and Plasma generation internal losses:

The GM assembly for the system includes two pumps: a small DC pump consuming 2 W and a vacuum pump consuming 300 W. All energy consumed by these pumps is supplied entirely by the solar PV system, with no input from the grid. It is important to note that the vacuum pump is oversized for the current flow rate, as it can support a much larger system

For the current small-scale experimental setup, the energy efficiency of blue hydrogen production may seem unfavorable, but this is only the case because some components are scaled up and others remain benchtop scale. Based on initial calculations, at a CH_4 flow rate of 64 sccm, it would take approximately 1.4 years of continuous operation to produce 1 kg of H_2. Over this period, both pumps would run continuously, leading to a significant power consumption of 302 W (combined for both pumps). This would result in the system consuming approximately 90 times more energy than the energy content of the H_2 produced. This highlights the need for more accurate estimates of energy consumption when the system is scaled up and optimized, which are provided below.

The plasma reactor currently operates at a flow rate of 64 sccm of CH_4, converting 25% of the input CH_4 to H_2 at the outlet. In its present configuration, the reactor's production rate is low, and continuous operation over the mentioned time frame is necessary to produce 1 kg of H_2. The vacuum pump is capable of handling 4,500 times the current H_2 flow rate, however, with only a <1% change in the pressure difference across the membrane, running at 200 W. At this optimized flow rate, the production of 1 kg of H_2 would take just 165 minutes.

For the membrane module in an optimized system, 22 DC pumps would be required running in parallel, although a larger and more efficient DC pump would significantly reduce energy consumption. This would bring the total power requirement for the membrane module to around 0.67 kWh/kg of H_2, when accounting for both the vacuum pump and the parallel DC pumps. Furthermore, in the scaled-up system, 4,500 plasma reactors (or one larger, optimized reactor) would be needed to match the vacuum pump’s capacity. The current DC pump is also significantly oversized, leading to unnecessary energy consumption. Table 1 outlines the key differences in energy requirements, flow rates, and overall efficiency between the experimental small-scale setup and a typical commercial H_2 production system.

Table 7.1. Comparison of energy consumption and efficiency metrics between small-scale and commercial hydrogen production systems

Parameter	Small-Scale System	Optimized Industrial-scale System
Biogas Flow Rate	64 sccm	64 sccm
Hydrogen Production Rate	25% of CH_4 input	25% of CH_4 input
Time to Produce 1 kg of H_2	1.4 years (continuous)	165 minutes
DC Pump Power Rating	2 W	44 W
Number of DC Pumps Required	1 (oversized)	22 DC pumps (optimized)
Total Pump Power Consumption	300 W (vacuum pump) + 2 W (DC pumps)	200 W (vacuum pump) + 44 W (DC pumps)
Energy Consumption by GM (per kg of H_2)	60.3 kWh	0.67 kWh
Number of Plasma Reactors Required	1	4500 plasma reactors (or optimized)
Energy Consumption	585 kWh	585 kWh
Time required	1.4 years	165 min

The total energy required for producing 1 kg of hydrogen using the plasma method is 585 kWh. This figure includes internal losses within the plasma generator, power consumed by the plasma reactor, and energy used for GM-based methane separation.

Water Requirements per kg of pale blue hydrogen:

The following points are noted while calculating water requirements per kg of pale blue hydrogen:

- The pale blue hydrogen consists **of Plasma produced blue hydrogen** and the **electrolyzer produced green hydrogen.**
- **The only water requirements are for the green hydrogen** hence the total water requirements for pale blue hydrogen are based on the water requirements for the green hydrogen only.

Calculation: Data provided by Cipher Neutron on their 5 kW system has shown that 90 g of hydrogen is produced per h and require ca. 1 litre/h of clean filtered water. For electrolysis therefore 1 Kg of green hydrogen (and by inference pale blue hydrogen) requires ca. 11 L of water per h. Assuming a (conservative) 65% efficiency of clean water recovery from an microalgae cultivation system, ca. 17 L of wastewater can be utilized to produce filtered and deionized water for the electrolyzer.

8 Conclusion and Recommendations

We have successfully integrated all of the components of the pale blue hydrogen project. The solution is ideal for rural areas to enable far more PV production than could be supported by the local loads if scaled.

It is recommended that future work is performed to :

- Integrate the technologies at the MW scale to the grid
- Optimize AEM operation
- Investigate partial financing FPV with water savings
- Complete an analysis of the economics of hydrogen – conversion to electricity vs other applications

Two membrane separation units were designed and constructed: (A) one for biogas separation into methane feed for the plasma reactor and carbon dioxide to be sequestered in the photobioreactor, and (B) a second to extract hydrogen downstream of the plasma reactor to recycle unreacted methane through the plasma system to improve yield. The possibility of using graphene membranes for this purpose was evaluated by comparison with commercial gas separation membrane options to select the most suitable membrane.

The hollow-fibre membrane units installed in the demonstration unit were measured to efficiently separate biogas, providing >99% purity methane at 30 sccm flow rate to the plasma reactor at a transmembrane pressure of 40 psi with a permeate pressure of 15 psi. The second membrane effectively extracted hydrogen produced in the plasma reactor, recycling a 95% pure unreacted methane stream back to the plasma reactor while operating with 15 psi transmembrane pressure. The membrane module had the necessary strength and stability to operate in the demonstration unit for several hours on multiple days.

To further improve the membrane separation unit effectiveness, we recommend that future designs employ multiple membrane stages within each membrane unit. For graphene membranes in particular, this approach would provide higher selectivity with less effort needed to enhance the material performance. Furthermore, multiple membrane stages would provide higher overall gas utilization.

During the membrane fabrication work, we mainly focused on using commercial support membranes beneath the graphene for permeance resistance matching to mitigate material defects. This leaves limited options for membrane structure and resistance, resulting in sub-optimal selections. It is recommended that future fabrication work use custom-synthesized polymer layers in the composite graphene membranes. This should provide more control over the support layer tuning to enhance overall membrane performance.

Commercially available compressors, particularly for hydrogen, are sized for significantly larger systems than the plasma reactor demonstration unit. As a result, the membrane and pump used in the design were oversized, and drew more power than was necessary. It is recommended that further plasma reactor scale-up efforts target a size where commercially available hydrogen compressor hardware could be taken advantage of in the membrane unit.

A reliable, durable plasma system for stable operation of CH_4 splitting reaction was successfully designed and established. This involves the combination of a gas supply and transport system, a plasma generator, a plasma reactor, and a product identification and analysis system. The core component of the plasma reactor was designed based on a dielectric barrier discharge (DBD) mechanism, and its operation was validated by the observed continuous H_2 production. Furthermore, the performance of the system was tuned by optimizing a series of technological parameters, including the length of the outer electrode, the voltage applied to the plasma reactor, the Argon concentration mixed with the input gas of CH_4, and the flowrate of the input gas. High CH_4 conversions of 30-75% were achieved under various experimental conditions. The energy consumption of H_2 production was optimized to as low as 585 kWh/kg H_2.

To further improve the CH_4 conversion and boost the H_2 production capability, a series of investigations regarding packing materials were conducted. These include the adjustment of the length of packing material, the location of packing material, and the type of packing material. Among these strategies, the use of catalytic W-Ni metals loaded on Al_2O_3-zeolite achieved a relatively high CH_4 conversion of 29%, although this performance is still imperfect compared with that without packing material (30%). To relieve the insulating effect of packing materials on plasma discharge, tuning their particle properties (e.g., particle size, microstructure, and morphology) is highly recommended for future research to improve the CH_4 conversion, with the aim of enhancing the interaction between the plasma field and the CH_4 molecules. In addition, development of highly efficient catalytic materials loaded on the packing materials is also necessary.

The solid byproduct generated from the CH_4 splitting reaction was validated as carbon material. This is consistent with the predicted splitting reaction. Solid carbon is useful for energy device applications (e.g., electrodes of lithium-ion batteries). However, the relatively low surface area of the obtained carbon material (8.2 m^2/g) could be caused by the agglomeration of the carbon particles during its interaction with the high-energy plasma field. Further chemical/physical treatments of the obtained carbon are necessary to achieve a surface area of at least tens of m2/g for practical applications.

Finally, the plasma system was integrated with a solar cell-charged power supply system and a graphene membrane-based gas separation system. The compatibility and stable operation of the overall system was successfully demonstrated, operating in an environmentally friendly and sustainable manner.

Future work is needed to integrate the scaled up versions of the photobioreactor, plasma reactor, and AEM electrolyzer to realize the pale blue hydrogen project at this intermediate scale. The same process that was demonstrated at the small bench top scale could be used for that integration.

Further, the FPV (and any other type of PV system) and AEM electrolyzer are both capable of being scaled up to the industrial and utility scales directly. This is also true of the other subsystems (photobioreactor) and plasma systems.

8 Lessons Learned

Several lessons were derived from the completed project.

- The complementary expertise of four different research leaders was very useful to amalgamate different concepts into a single milestone.
- The production of blue hydrogen at bench scale was successful however several questions were left unanswered. In terms of the techno-economics at large scale.
- The time line of one year for completing all aspects on this project was too compressed as there are unintended delays such as delays in procurement of supplies and equipment. Getting the necessary approval for operating outdoors is also a factor which needs to be taken into account. Construction of a solar green house on the algae pond was abandoned due to delays in getting approval to move aheaf.
- Inspite of the challenges, we learnt that it is possible to test and validate hypothesis over this short time line and we do want to thank IESO for supporting us in this ambitious project.
- The lessons learnt in this project will certainly open up opportunities for all the researchers and IESO to move forward to the next steps. We hope IESO considers going forward with some or all of the sub projects described herein.

10. Next Steps

- Investigate the integration of the system in more detail with supply of carbon dioxide to the photobioreactor and methane to the plasma system.
- The plasma-assisted CH_4 splitting system was found to be a disruptive technologiy an and offers great potential for blue hydrogen. The next steps should focus on solving the remaining issues:
    - Decrease of energy consumption: Current stage achieved an optimized energy consumption of 585 kWh/kg H_2 at a CH_4 conversion of 30 %. However, the obtained energy consumption value is still significantly higher than other mainstream H_2 production technologies, e.g., methane steam reforming (18.5 kWh/kg H_2) and water splitting (53 kWh/kg H_2). Lowering the energy consumption of the plasma-assisted CH_4 splitting to around 50-100 kWh/kg H_2 would make it competitive in the current market.
    - Optimization of input gas composition: Argon has been identified as a useful additive mixed with the input gas of CH_4 to enhance the excitation and ionization of CH_4 molecules in plasma. This took advantage of the relatively large molecules of Argon to enhance the plasma effect. However, the current issue is the lowered H_2 production rate when Argon was added. The use of other inert gases with different molecular sizes as the additive could be a meaningful research direction, with the aim of enhancing the plasma field and thus producing more H_2 under the same electrical input conditions.
    - Design of larger scale reactors : It has been found that the flowrate of CH_4 played a crucial role in CH_4 conversion. This is because the time duration of interaction between plasma field and CH_4 molecules can be changed by using different flowrate. Inspired by this, if a larger reactor can be designed with a larger active volume for gas flow, the H_2 production will be increased with the same gas flowrate. However, the energy density may be changed thus leading to an adverse effect. Optimization of the overall effect deserves future research.
    - Development of efficient packing materials: The adding of packing material may influence the plasma field to improve the interaction between plasma and the CH_4 molecules. Development of efficient packing materials involves two major directions: I. Optimization of the properties (particle size, microstructure, and morphology) of existing packing materials; II. Design of new, efficient catalytic materials loaded on packing materials. These strategies could tune the plasma discharge property and relieve the intrinsic insulating property of packing materials (e.g., Al_2O_3). Furthermore, the interaction mechanism between packing materials and the plasma field will be clarified in detail.

Appendix 1

Video record on demonstration at ICFAR Western University field site

A preview video overview of the Pale Blue Hydrogen Project: https://youtu.be/_6Ffc_47W0o

A detailed master class video going into detail on each subsystem: https://youtu.be/dSGYTt3C1RQ

Appendix 2 Research Questions

	Blue Hydrogen	Green Hydrogen	Comments
Cost	Higher infrastructure and operating costs due to the complex process requirements. Energy input is significant unless coupled with PV or other renewables,	The major cost is for the purification and use of water . 1 KG /h of Green hydrogen requires ca. 11 L/h of filtered, deionized water. PV-AEM systems can lower energy costs.	By combining both blue and green hydrogen leads to significant savings in water costs and carbon deficit.
Likelihood	Further work is needed on scaleup of the plasma system	There is a large likelihood of adoption of this technology in the near future	
Emissions	Emissions are very low under efficient operation of the plasma reactor as carbon black is a product. By combining microalgae capture of carbon dioxide and sequestration in eco - plastics will minimize any carbon emission	There is no emission of carbon dioxide in this process if PV systems are used as energy source.	LCA reveals that the upstream processing of PV panels will generate CO_2 emissions
Imports vs domestic	Biogas is a readily available source from digesters, landfills and natural gas (methane)	The manufacture of AEM electrolyser systems is a growing	There is no requirement for imports due to the large resource base in Canada
Infrastructure	Biogas source; pumps, mixers, compressors. Storage tanks piping, plasma reactor, membranes for gas separation	Water storage, water purifier. PV panels, Electrical network panels, AEM elecrolyzer, compressor, gas storage	Green hydrogen system have a simpler plant layout; the water requirements can be an issue with scaled up systems